Stoten, D. P. (2017). A comparative study and unification of two methods for controlling dynamically substructured systems. *Earthquake Engineering and Structural Dynamics*, *46*(2), 317–339. https://doi.org/10.1002/eqe.2797

A comparative study and unification of two methods for controlling dynamically substructured systems

David Paul Stoten*,†

Advanced Control and Test Laboratory (ACTLab), Department of Mechanical Engineering, University of Bristol, Bristol, BS8 1TR, UK

SUMMARY

This paper addresses the problem of advanced testing of systems via the principle of dynamic substructuring. Use is made of the hybrid simulation (HS) scheme framework to develop a new method of synthesis for the dynamically substructured system (DSS) scheme of Stoten and Hyde; [1]. Principal reasons for doing this are (i) to improve upon the original method of DSS synthesis by adopting the more intuitive framework of HS and (ii) to enable the amalgamation of HS and DSS into a unified substructured system (USS) scheme, so that the significant advantages of DSS can be incorporated into an existing HS scheme as a straightforward retrofit.

Having established the common framework for HS/DSS the paper also illustrates, by way of an example, compensator/controller synthesis for the two schemes, together with their advantages and disadvantages. In doing this both schemes are retained in their basic forms, i.e. there are no additional control embellishments used in this work, such as delay compensation, adaptive control or other advanced control methods. In order to maintain as much transparency as possible, use is made of well-known classical control techniques. Common problems associated with the substructure testing technique are also investigated, including the effects of physical parameter uncertainty, pure delays in signals and a 'split-mass' in the substructure formulation. It is shown that, although the new formulation of controlled-DSS requires more design effort than compensated-HS, the advantages of DSS in terms of stability and robustness significantly outweigh this small disadvantage at the design stage.

KEY WORDS: Dynamic substructuring, automatic control, advanced testing.

1. INTRODUCTION

Ever since the latter years of the last century, the concept and design of dynamically substructured methods of system testing have received significant interest from academic researchers, test institutions and industry. The ideal objective of this form of advanced testing has remained more-or-less the same since its inception: to test physically full-size components of a complete (emulated) system, as if those components were *in situ*. Elements of the emulated system that are not part of the physical test are represented by a real-time numerical simulation, which must be executed in parallel with the physical component test. Ideally, exact synchronisation of the physical and numerical elements (i.e. substructures) at their interfaces is required, so that the combined substructures generate responses that exactly match those of the emulated system.

The method of substructure testing is an intuitively sound concept, but there are potential pitfalls in realising the above ideal objective, some of which are as follows:

(i) The necessity for additional actuation and sensing of the physical substructures.
(ii) Parameter and structural uncertainty of the physical substructures and the actuation systems. Such uncertainty will often occur in the physical system under test; for example, changes in stiffness and damping coefficients under extreme loading conditions. Significant parameter uncertainty can also be present in the actuation system(s), especially if the frequency and amplitude ranges of the test signal are relatively large.

---

*Correspondence to: David Paul Stoten, ACTLab, Department of Mechanical Engineering, University of Bristol, University Walk, Bristol BS8 1TR, UK.
†E-mail: d.p.stoten@bristol.ac.uk

(iii) Numerical substructures with large dimensionality and complexity, which can be difficult to simulate in real-time.
(iv) Pure delays in signal communications between substructures, most likely due to the use of discrete-time computational devices and any significant transmission distances.
(v) The necessity for stable, robust controllers that can guarantee excellent synchronisation of the substructures at their interfaces, despite the presence of (i)-(iv).
(vi) Controller design issues in (v), for example, the complexity of the control synthesis technique.

One of the earliest attempts at solving the substructuring problem was via the method of hybrid simulation, sometimes referred to as real-time pseudo-dynamic testing, the hybrid method or the hybrid scheme (HS); [2]. This method and developments of it continue to be used with success, particularly in tests that have relatively low bandwidth dynamics and where dynamic uncertainty is not a major issue; [3], [4]. When compared with alternative techniques, the principle advantage of HS, in its basic form, is the relatively simple strategy of inverse-dynamics *compensator* design and implementation. However, the principle disadvantage of HS is its inherent lack of robustness to parameter uncertainty and communication delays. Specifically, lightly damped emulated systems, such as civil engineering structures, can result in the implementation of unstable HS-based test systems.

Key to the success of HS is the accuracy of the dynamic model of the physical substructure's actuator, since it is the inverse of this model that forms the basis of the compensator design. Some of the earlier approaches to HS design assumed an actuator model to be a pure time delay (e^{-Ts}, where T is the delay time), so that approximate delay compensation methods were used in an attempt to provide the necessary cancellation; [3], [7]-[9]. However, this choice of model is counter to standard engineering practice, where typical servohydraulic or electrical actuators, together with their inner-loop controllers, are conventionally modelled as polynomial transfer functions. For example, a step input to a pure delay system would generate an output that is the same step delayed by T seconds. This is never the case in practice, where actuator (step) responses exhibit exponential/sinusoidal transient components; e.g. Figure 6 in [7] shows a recorded plot of this type of actuator response. However precise the delay compensation method, the dynamics of the real actuator will never be adequately cancelled, resulting in the implementation of inaccurate and even unstable HS schemes.

Realisation of these problems lead later investigators to use standard models of actuator polynomial transfer functions, in series with a pure delay term having a smaller value of T than had previously been used; [10]-[12]. Effectively, the pure delay now correctly modelled the discrete-time nature of the actuator inner-loop controller. Hence, these later methods required the HS compensator to possess two types of cancellation: one for the transfer function and one for the pure delay. However, even if the compensator can approximately cancel the real actuator dynamics, the HS scheme *per se* can be significantly limited in terms of its stability and robustness, as is shown in §3.

In more recent years an alternative to HS has been developed, called the dynamically substructured system (DSS) scheme, the main motivation being to improve upon the levels of stability and robustness offered by the HS scheme; [1], [13]. This has been achieved by establishing a different, perhaps less intuitive, substructuring framework from that of HS and using this new framework to synthesise a synchronising *automatic controller*, based upon a conventional transfer function approach. Implementation tests of DSS have verified the improvements in both stability and robustness that can be achieved by this method; [14]-[16]. Moreover, the synthesis and implementation of a state-space version of DSS has been shown to be a relatively straightforward exercise, resulting in the DSS synchronisation of multivariable substructuring problems and a test for 'substructurability', similar to the matrix rank test for controllability; [17].

Arguably, the original design of the DSS synchronising controller is a less intuitive and more demanding task than the design of the inverting compensator for HS. For this reason, one of the principle objectives of this current work is to use the HS framework for the synthesis of DSS controllers, enabling a unified substructured system (USS) approach. A significant advantage of

USS is that it permits a straightforward retrofit of the new DSS approach onto an existing HS implementation, a technique that is also described here.

The content in this paper is occasionally of a didactic nature and this is evident in §2, a brief description of the underlying substructured dynamics framework that will be used throughout the remaining sections. §§3, 4 present the common HS and DSS frameworks, together with the respective compensator and controller synthesis methods. §5 then briefly describes the USS framework and the method of DSS retrofit control. A simulated example of a substructured system and its compensator/controller design and performance is presented in §6-8. Although of a specific nature, the example has been designed to illustrate the following general features that can cause stability and robustness problems in practical test systems:

- The interface between substructures lies within an inertial component (the so-called 'split-mass' problem; [18]-[21]).
- Parameter uncertainty can exist within the physical substructure and the actuator.
- A pure delay can exist in the actuator and compensator/controller (collectively known as the transfer system), due to the discrete-time nature of some the hardware.

In §§3-8, both the HS compensator and DSS controllers are presented in their most basic formats, in order to allow for balanced comparisons between the methods of design, the analytic and simulated results and the advantages and disadvantages of each approach. For example, there are no embellishments such as delay compensation, adaptive control and self-tuning control included in this work. Finally, the main conclusions are presented in §9.

2. SUBSTRUCTURED DYNAMIC SYSTEMS

Consider a generalised form of substructured system as shown in Figure 1. At the top of the figure is an emulated system (Σ_E), with serial multi - degree-of-freedom (DOF) dynamics that are assumed to be linear and comprised of inertial, conservative and dissipative components. Motion is constrained to the horizontal direction and disturbances, $\{d_1, d_2\}$, are applied to the system resulting in a displacement, y, at an arbitrarily defined interface. This interface represents the boundary between the multi-DOF numerical and physical substructures, arbitrarily selected as Σ_1 and Σ_2 respectively, as shown at the bottom of the figure. Displacements of $\{\Sigma_1, \Sigma_2\}$ at the interface are y_1 and y_2 , whilst the interface (constraint) force is f.

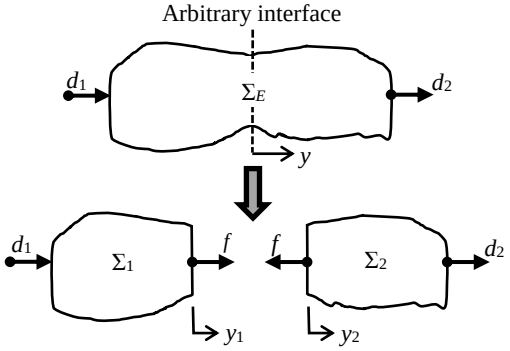

Fig. 1 A generalised emulated system, Σ_E, and its associated substructured systems, $\{\Sigma_1, \Sigma_2\}$.

The principle requirement of $\{\Sigma_1, \Sigma_2\}$ is that their dynamical behaviour is identical to that of Σ_E at the interface, so ideally:

$$y_1(s) = y_2(s) = y(s) \tag{1}$$

where s is the Laplace complex frequency operator (omitted from dynamic function and signal arguments in most of what follows, for the sake of brevity). The forward dynamics of Σ_E can therefore be written as:

$$y = G_{E1}d_1 + G_{E2}d_2 \tag{2}$$

where G_{E1} and G_{E2} are transfer functions of Σ_E. Similarly, the forward dynamics of Σ_1 are:

$$y_1 = G_{d1}d_1 + G_1 f \tag{3}$$

whilst the inverse dynamics of Σ_2 are:

$$f = G_{d2}d_2 + G_2 y_2 \tag{4}$$

Assuming that (1) is satisfied, (2)-(4) imply that Σ_E can be represented by its substructures, $\{\Sigma_1, \Sigma_2\}$, in the quasi closed-loop form of Figure 2.

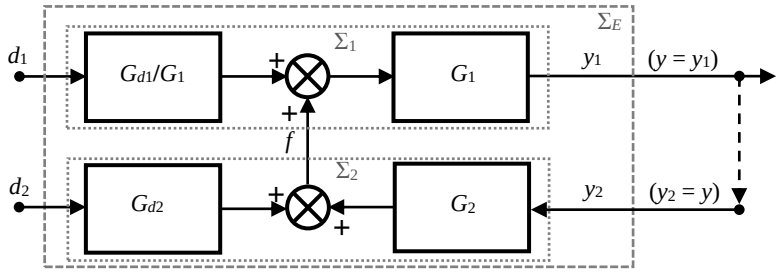

Fig. 2 Σ_E showing the $\{\Sigma_1, \Sigma_2\}$ components in a quasi closed-loop form.

Assuming that the dashed arrow in Figure 2 symbolically closes the loop, Σ_E can be written as:

$$y = \underbrace{\left(\frac{G_{d1}}{1-G_1G_2}\right)}_{G_{E1}} d_1 + \underbrace{\left(\frac{G_1G_{d2}}{1-G_1G_2}\right)}_{G_{E2}} d_2 \tag{5}$$

In §3 the aim is to investigate a typical hybrid scheme (Σ_{HS}) synthesis that ensures physical closure of the loop between y_1 and y_2 in Figure 2, and also to examine the advantages and disadvantages of this scheme. Then an alternative to Σ_{HS}, the dynamically substructured system (Σ_{DSS}) scheme, is presented in §4.

3. COMPENSATION OF HYBRID SYSTEMS

An idealised Σ_{HS} can be synthesised directly from Figure 2 by ensuring physical closure of the loop via the introduction of an actuator and compensator, G_A and G_C respectively, into the feedback path. The combination of the actuator and compensator is known as the transfer system, Σ_{TS}, which is shown within the resulting Σ_{HS} of Figure 3. An approach to compensator design is to ensure that the following relationship is satisfied, where $\hat{G}_A$ is an estimate of the actuator transfer function; [10], [13]:

$$G_C = \hat{G}_A^{-1} \tag{6}$$

Hence, assuming complete parameter certainty, the synthesised Σ_{HS} is identical to Σ_E, so that the characteristic polynomial (CP) of Σ_{HS} will be the same as that of Σ_E, namely $(1 - G_1G_2)$ from (5).

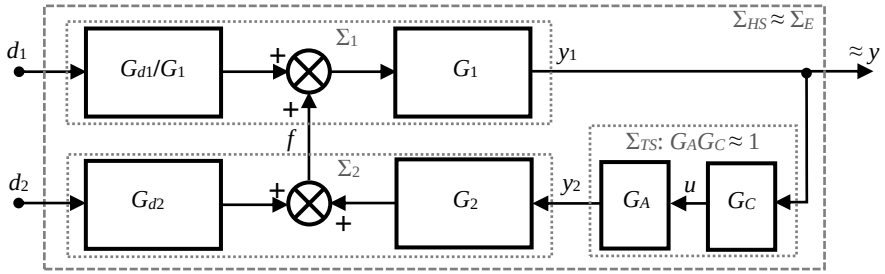

Fig. 3 Σ_{HS} in closed-loop form with an actuator, G_A, and compensator, G_C.

However, the most significant problems with this approach are:

(i) Since the CPs associated with Σ_E and Σ_{HS} are identical, the corresponding roots of their common characteristic equation (CE):

$$1 - G_1 G_2 = 0 \tag{7}$$

will also be identical. If Σ_E is lightly damped, e.g. less than ~10%, the roots will be relatively close to the imaginary axis of the *s*-plane. Uncertainty of the dynamic parameters within Σ_2 and also the actuator component of Σ_{TS} ensure that $G_A G_C \neq 1$, often leading to a migration of closed-loop characteristic equation (CLCE) roots further towards the imaginary axis. In turn, this leads to a loss of relative stability and even to instability, should any roots cross the axis into the right-half *s*-plane.

(ii) Moreover, the relative degree of G_A will generally be $r > 0$, so that G_C will be improper according to (6). In order to avoid the problem of having to generate noise-sensitive derivatives of y_1 , G_C will often have its denominator padded with additional dynamics, $(1 + \varepsilon s)^r$, where $\varepsilon > 0$ is sufficiently small. However, this modification will also decrease the relative stability of the HS system by increasing the phase lag around the loop.

(iii) In addition, pure delay terms can often exist in Σ_{TS} , due to any discrete-time elements within the inner-loop controller (considered to be part of the actuator dynamics, G_A) and also within the compensator, G_C. The aggregate of such pure delays, typically in the order of milliseconds, will inevitably lead to a loss of phase between y_1 and y_2; again, the consequence will be a reduction in relative stability and hence an increase in the potential for instability.

In these circumstances, more representative forms of Σ_{HS} closed-loop transfer functions (CLTF) are given by the expressions in (8), which will be approximately equal to G_{E1} and G_{E2}:

$$y_1 = \underbrace{\left(\frac{G_{d1}}{1 - G_A G_C G_1 G_2} \right)}_{\approx G_{E1}} d_1 + \underbrace{\left(\frac{G_1 G_{d2}}{1 - G_A G_C G_1 G_2} \right)}_{\approx G_{E2}} d_2 \tag{8}$$

and therefore, even if stability is preserved, $y_1 \neq y$.

Without any further enhancement to the form of compensation described, such as delay compensation or self-tuning control, it is concluded that Σ_{HS} lacks inherent robustness to the presence of parameter uncertainty within $\{\Sigma_2 , \Sigma_{TS}\}$ and to pure delays created by any discrete-time computational elements within Σ_{TS}. Therefore, a prime objective of this work is to devise a method based upon the principles of automatic control that builds upon the intuitive framework of Σ_{HS}, but yields significant improvements in stability and robustness. This will be achieved by ensuring that the new method has a CL error CE (CLECE), which is different from the CLCE of Σ_{HS} and whose roots can be arbitrarily assigned via well-known methods of control system design. Separately, the overall objective of synchronising y_2 with y_1 , whilst emulating the behaviour of Σ_E, will also be satisfied. In order to do this, the concept of DSS and their control is introduced and described in §4.

4. AUTOMATIC CONTROL OF DYNAMICALLY SUBSTRUCTURED SYSTEMS

The new approach taken in this section revisits the Σ_{DSS} method of Stoten and Hyde [1], incorporating the Σ_{HS} framework as the starting point for the automatic controller design. One of the objectives in doing this is to provide a unified substructured system (Σ_{USS}) and control methodology, i.e. to synthesise a common framework for Σ_{HS} and Σ_{DSS} design. A practical advantage of this new approach is that it will allow the retrofit of a Σ_{DSS} control loop into an existing Σ_{HS} implementation, in order to improve the accuracy and robustness of the substructured test.

Hence, with the structure of Σ_{HS} shown in Figure 3 and reference [1] acting as guides, the following linear substructuring controller (LSC) is proposed for the new Σ_{DSS} configuration:

$$u = K_e e + K_{d1} d_1 + K_{d2} d_2 ; \quad e = y_1 - y_2 \tag{9}$$

where *e is* the synchronisation error and $\{K_e, K_{d1}, K_{d2}\}$ are feedback and feedforward control transfer functions. Figure 3 is thereby transformed into the Σ_{DSS} shown in Figure 4.

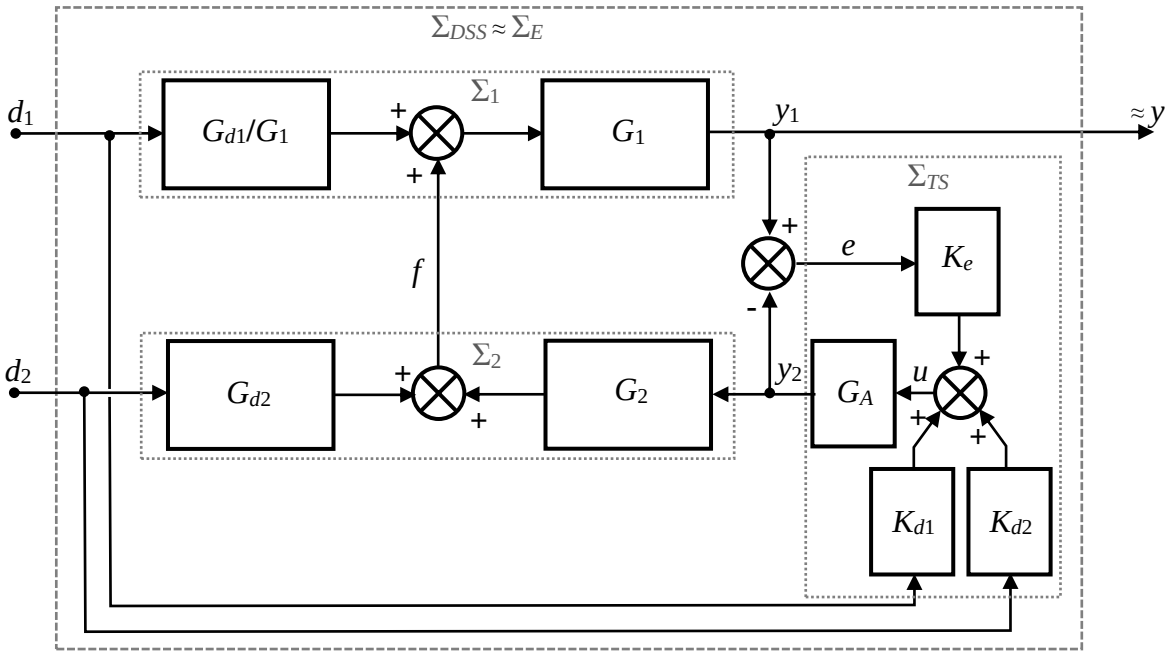

Fig. 4 Σ_{DSS} based upon the amalgamation of the Σ_{HS} formulation of Figure 3 and reference [1].

From Figure 4:

$$y_1 = G_1\left(\frac{G_{d1}}{G_1}d_1 + G_{d2}d_2 + G_2G_Au\right);\ \ y_2 = G_Au \tag{10}$$

so that (9) and (10) yield the closed-loop error dynamics:

$$e = \left(\frac{G_{d1} - G_A(1-G_1G_2)K_{d1}}{1+G_A(1-G_1G_2)K_e}\right)d_1 + \left(\frac{G_{d2}G_1 - G_A(1-G_1G_2)K_{d2}}{1+G_A(1-G_1G_2)K_e}\right)d_2 \tag{11}$$

Assuming complete parameter certainty, solutions for the feedforward gains that ensure $e \to 0$ are provided by (11):

$$K_{d1} = \frac{G_{d1}}{G_A(1-G_1G_2)} \text{ and } K_{d2} = \frac{G_{d2}G_1}{G_A(1-G_1G_2)} \tag{12}$$

Robustness of the Σ_{DSS} error dynamics in the presence of parameter uncertainty can then be ensured by suitable design of K_e, using the CLECE inferred from (11) as the basis for this design:

$$1+G_A(1-G_1G_2)K_e = 0 \tag{13}$$

Comparing (13) with (7), it is evident that a suitable design of K_e permits arbitrary selection of the CLECE roots of the Σ_{DSS} - a result that is in sharp contrast to the simpler design outcome from Σ_{HS}, which offers no such possibility.

In addition, it is now shown that the CL response of Σ_{DSS} (relating y_1 to d_1 and d_2) in Figure 4 matches the equivalent response of Σ_E, independently of the design of the stabilising K_e. In the following, it is assumed that $e \neq 0$ for the sake of generality. Thus, (9) and the second part of (10) yield:

$$u = \left(\frac{K_e}{1+K_eG_A}\right)y_1 + \left(\frac{K_{d1}}{1+K_eG_A}\right)d_1 + \left(\frac{K_{d2}}{1+K_eG_A}\right)d_2 \tag{14}$$

so that the first part of (10) together with (14) yield the CL response of Σ_{DSS} as:

$$y_1 = \left[\frac{G_{d1} + G_AG_{d1}K_e + G_AG_1G_2K_{d1}}{1+G_A(1-G_1G_2)K_e}\right]d_1 + \left[\frac{G_1(G_{d2} + G_AG_{d2}K_e + G_AG_2K_{d2})}{1+G_A(1-G_1G_2)K_e}\right]d_2 \tag{15}$$

Substitution of the solutions for the forward gains from (12) into (15) ultimately yields the equivalence of Σ_{DSS} and Σ_E:

$$y_1 = \left[\frac{G_{d1}[1+G_A(1-G_1G_2)K_e]}{(1-G_1G_2)[1+G_A(1-G_1G_2)K_e]}\right]d_1 + \left[\frac{G_1G_{d2}[1+G_A(1-G_1G_2)K_e]}{(1-G_1G_2)[1+G_A(1-G_1G_2)K_e]}\right]d_2$$

since, on cancellation of $1+G_A(1-G_1G_2)K_e$ in the above equation, it is revealed that Σ_{DSS} possesses an identical pair of CLTF to those defined for Σ_E in (5), i.e. G_{E1} and G_{E2}:

$$y_1 = \underbrace{\left(\frac{G_{d1}}{1-G_1G_2}\right)}_{G_{E1}}d_1 + \underbrace{\left(\frac{G_1G_{d2}}{1-G_1G_2}\right)}_{G_{E2}}d_2 \tag{16}$$

Thus, the crucial aspect of the Σ_{DSS} design approach can be stated as follows (assuming parameter certainty for the present):

(a) Equation (16) implies that the LSC forces Σ_{DSS} to have a CL dynamic response that is identical to the response of Σ_E, with both systems having their fixed CLCE roots given by $1-G_1G_2=0$.

(b) However, from (11), the synchronisation error dynamics of Σ_{DSS} are governed by the entirely separate CLECE, $1+G_A(1-G_1G_2)K_e=0$, with roots that can be arbitrarily assigned by suitable design of K_e.

(c) Hence, (a) and (b) imply that Σ_{DSS} possesses arbitrary (but finite) levels of stability and robustness of its error dynamics, whilst retaining a fixed CL response dynamic matching that of Σ_E.

The example described in §§6-8 further amplifies points (a)-(c) in a quantitative manner. In addition, the effects of physical parameter uncertainty and pure delays, for both Σ_{HS} and Σ_{DSS}, are also examined by way of this example.

5. UNIFIED SUBSTRUCTURED SYSTEMS

Straightforward integration of Σ_{HS} with the new Σ_{DSS} design leads to a unified substructured system (USS; Σ_{USS}) method of control. The main motivation for this is a practical one - to improve the stability and robustness of an existing (probably hardwired) implementation of Σ_{HS}, via the addition of a Σ_{DSS} retrofit loop. There are at least two possible solutions to this problem, termed pre-Σ_{HS} and post-Σ_{HS} retrofit strategies, which are described below.

The pre-Σ_{HS} strategy is shown in Figure 5, where the summing junction for the additional Σ_{DSS} control signal is placed before the Σ_{HS} compensator, G_C. The objective is to ensure that u in Figure 5 is identical to the original Σ_{DSS} control signal, via the action of the Σ_{USS} gains, $\{K_{d11}, K_{d22}, K_{e1}, K_{e2}\}$. Comparing the expression for u from Figure 5 with that generated by the Σ_{DSS} controller alone, yields:

$$u = G_C[K_{d11}d_1 + K_{d22}d_2 + (K_{e1}+1)y_1 - K_{e2}y_2] = K_{d1}d_1 + K_{d2}d_2 + K_e y_1 - K_e y_2 \tag{17}$$

so that the Σ_{USS} gains are simply given by:

$$K_{d11} = \frac{K_{d1}}{G_C};\ K_{d22} = \frac{K_{d2}}{G_C};\ K_{e1} = \frac{K_e}{G_C} - 1;\ \ K_{e2} = \frac{K_e}{G_C} \tag{18}$$

The advantages of this particular retrofit strategy are that all of the original Σ_{DSS} gains are modified by the inverse of G_C ($\approx G_A$) and therefore the expressions in (18) remain proper or strictly proper. However, a potential disadvantage is that access to the summing junction may not be feasible in an existing, hardwired Σ_{HS} implementation.

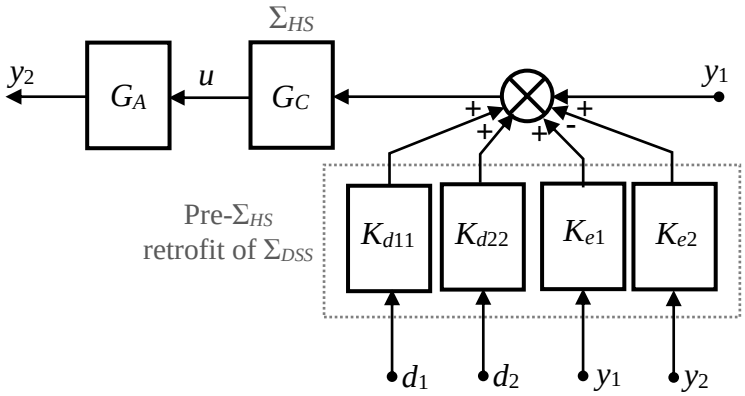

Fig. 5 Σ_{USS}: pre-Σ_{HS} retrofit of Σ_{DSS}.

The alternative post-Σ_{HS} strategy is shown in Figure 6, where the summing junction is now placed immediately after the compensator and the new retrofit gain set is described by$\{K_{d11}, K_{d22}, K_{ec}, K_e\}$. Again, comparing the expression for u in Figure 6 with that generated by the Σ_{DSS} controller alone, yields:

$$u = K_{d1}d_1 + K_{d2}d_2 + (K_{ec} + G_C)y_1 - K_e y_2 = K_{d1}d_1 + K_{d2}d_2 + K_e y_1 - K_e y_2 \tag{19}$$

Hence the only modification required to the original Σ_{DSS} gain set is to the K_e term operating on y_1:

$$K_{ec} = K_e - G_C \tag{20}$$

The obvious advantage of this method is that K_{d1}, K_{d2} and K_e (for y_2) are preserved from the original Σ_{DSS}-LSC design. In addition, placing the summing junction prior to the actuator is likely to be a more feasible proposition than it was in the previous case. However, a disadvantage is that the expression for K_{ec} in (20) is likely to be non-proper, so that padding of the denominator will be required using the same method as described in §3.

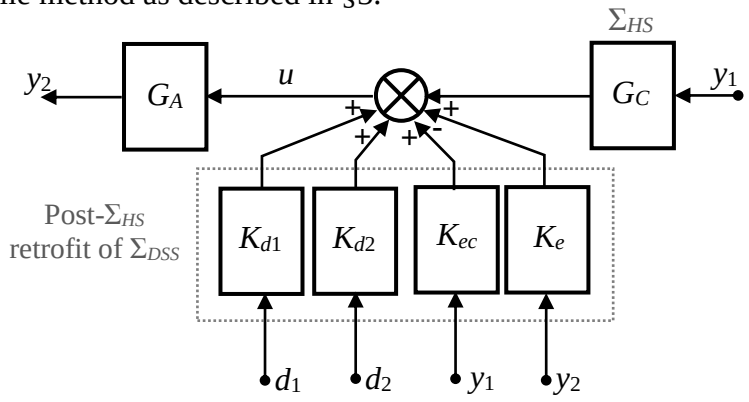

Fig. 6 Σ_{USS}: post-Σ_{HS} retrofit of Σ_{DSS}.

6. AN EXAMPLE

The purpose of this section is to present an example of dynamic substructuring that will be used in §§7, 8 to illustrate, in a quantitative manner, (i) the processes involved in both Σ_{HS} and Σ_{DSS} controller designs; (ii) the efficacy of the designs in terms of synchronisation performance of the substructures,$\{\Sigma_1, \Sigma_2\}$; (iii) the efficacy of the designs in terms of Σ_E-tracking; (iv) the advantages and disadvantages of the designs.

Key substructuring and control problems that were described in §1 will be addressed here, too: the 'split-mass' problem, the effects of uncertainty in physical parameters and the effects of a pure delay term in the dynamics. In keeping with the didactic nature of some of this work, the approach to control design is relatively straightforward; classical control engineering techniques are used, including the Evans roots' loci plot, the polar plot and the Nyquist stability criterion; [22].

Although of a specific nature, the example is nevertheless of sufficient generality to highlight key features of typical substructuring problems and their control, but without the encumbrance of excessively large dimensionality and dynamic complexity. In particular, Σ_E is a linear, serially-connected dynamic system with 3-DOF and $\{\Sigma_1, \Sigma_2\}$ each have 2-DOF, with uncertainty in their physical parameters. Thus, Σ_E is the mass-spring-damper arrangement with parameters m, k, and c, shown at the top of Figure 7. A single external displacement disturbance, d_2 (= d) is applied to the right-hand extremity of the system, whilst the left-hand extremity is constrained to be stationary ($d_1 = 0$). The resulting $\{\Sigma_1, \Sigma_2\}$ are shown at the bottom of Figure 7, where the adjustable interface is chosen to lie within the second mass, so that $m_1 + m_2 = 3m$ and $0 \le m_1 \le 3m$. The interaction (constraint) force between the substructures is f and arbitrarily Σ_1 is selected as the numerical substructure and Σ_2 as the physical substructure. The interface location is also arbitrary and will often be chosen pragmatically, being based upon the natural boundary between a physical test specimen and the numerical substructure. For example, an alternative location in Figure 7 might be at 'A' and although the dynamics of $\{\Sigma_1, \Sigma_2\}$ will change, the resulting developments will be very similar to those presented here.

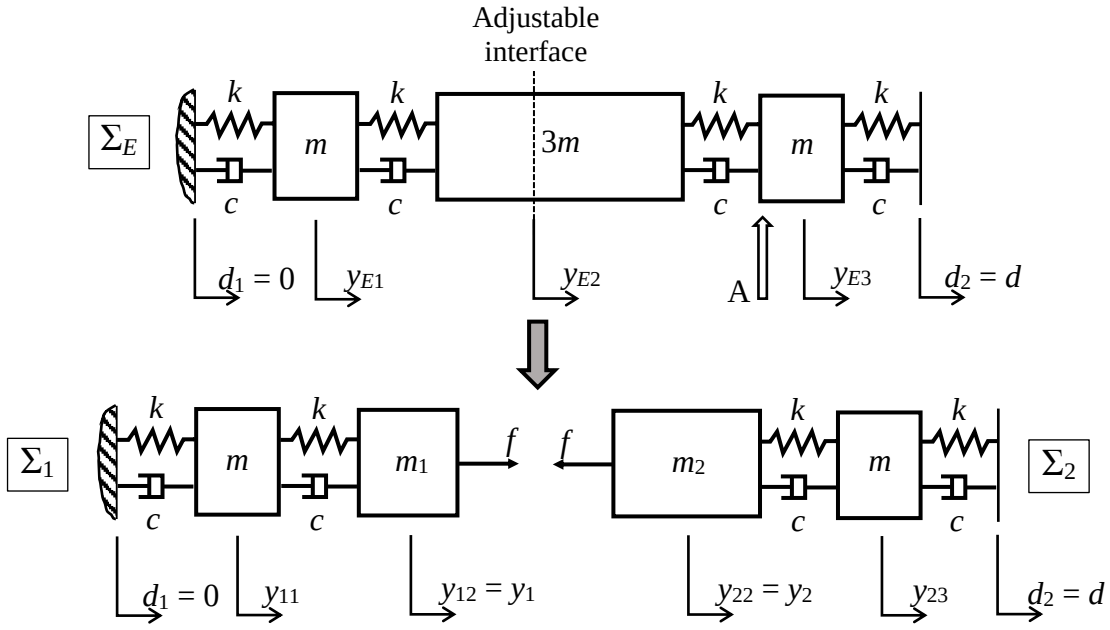

Fig. 7 The emulated system, Σ_E (top) and the 2 substructures $\{\Sigma_1, \Sigma_2\}$ (bottom); Σ_1 is the numerical substructure and Σ_2 is the physical substructure.

Hence the dynamics of Σ_E in the time domain are given by:

$$\left\{\begin{array}{c} -ky_{E1} - c\dot{y}_{E1} + k(y_{E2} - y_{E1}) + c(\dot{y}_{E2} - \dot{y}_{E1}) = m\ddot{y}_{E1} \\ -k(y_{E2} - y_{E1}) - c(\dot{y}_{E2} - \dot{y}_{E1}) + k(y_{E3} - y_{E2}) + c(\dot{y}_{E3} - \dot{y}_{E2}) = 3m\ddot{y}_{E2} \\ -k(y_{E3} - y_{E2}) - c(\dot{y}_{E3} - \dot{y}_{E2}) + k(d - y_{E3}) + c(\dot{d} - \dot{y}_{E3}) = m\ddot{y}_{E3} \end{array}\right\} \tag{21}$$

and the dynamics of Σ_1 are:

$$\left\{\begin{array}{c} -ky_{11} - c\dot{y}_{11} + k(y_{12} - y_{11}) + c(\dot{y}_{12} - \dot{y}_{11}) = m\ddot{y}_{11} \\ -k(y_{12} - y_{11}) - c(\dot{y}_{12} - \dot{y}_{11}) + f = m_1\ddot{y}_{12} \end{array}\right\} \tag{22}$$

so that the forward dynamics of Σ_1 in the Laplace (complex frequency) domain are:

$$y_{12} = y_1 = \underbrace{\left[\frac{ms^2 + 2cs + 2k}{(m_1 s^2 + cs + k)(ms^2 + 2cs + 2k) - (cs + k)^2}\right]}_{G_1} f = G_1 f \tag{23}$$

Similarly, the dynamics of Σ_2 are:

$$\left\{\begin{array}{c} k(y_{23}-y_{22})+c(\dot{y}_{23}-\dot{y}_{22})-f=m_2\ddot{y}_{22} \\ -k(y_{23}-y_{22})-c(\dot{y}_{23}-\dot{y}_{22})+k(d-y_{23})+c(\dot{d}-\dot{y}_{23})=m\ddot{y}_{23} \end{array}\right\} \tag{24}$$

so that the inverse dynamics of Σ_2 are:

$$f=\underbrace{\left[\frac{-(m_2s^2+cs+k)(ms^2+2cs+2k)+(cs+k)^2}{ms^2+2cs+2k}\right]}_{G_2}\underset{y_2}{y_{22}}+\underbrace{\left[\frac{(cs+k)^2}{ms^2+2cs+2k}\right]}_{G_{d2}\,(=G_d)}d=G_2y_2+G_dd \tag{25}$$

Polynomials within the substructure transfer functions $\{G_1, G_2, G_{d2} (= G_d)\}$, as defined in (23) and (25) are now written as:

$$\left\{\begin{array}{c} p_{11}=ms^2+2cs+2k \\ p_{12}=(m_1s^2+cs+k)(ms^2+2cs+2k)-(cs+k)^2 \\ p_{21}=(m_2s^2+cs+k)(ms^2+2cs+2k)-(cs+k)^2 \end{array}\right\} \tag{26}$$

so that:

$$G_1=\frac{p_{11}}{p_{12}};\quad G_2=\frac{-p_{21}}{p_{11}};\quad G_d=\frac{(cs+k)^2}{p_{11}} \tag{27}$$

Hence the substructured system is as shown in Figure 2, where the output of Σ_1 is now written as $y_1 = y_{12}$ and the input to Σ_2 as $y_2 = y_{22}$.

In order to represent a lightly damped structure with natural frequencies of less than ~3Hz, nominal values of the parameters are chosen as m = 100 kg, k = 10000 N/m and c = 20 Ns/m, so that from (26) and (27), the dynamics of the substructures are given by:

$$\left\{\begin{array}{l} \Sigma_1:\ G_1=\dfrac{p_{11}}{p_{12}}=\dfrac{100s^2+40s+2\times10^4}{2\times10^4s^4+10^4s^3+5.0004\times10^6s^2+4\times10^5s+10^8} \\ \Sigma_2:\ G_2=\dfrac{-p_{21}}{p_{11}}=\dfrac{-(10^4s^4+6\times10^3s^3+3.0004\times10^6s^2+4\times10^5s+10^8)}{100s^2+40s+2\times10^4} \\ \qquad G_d=\dfrac{(cs+k)^2}{p_{11}}=\dfrac{400s^2+4\times10^5s+10^8}{100s^2+40s+2\times10^4} \end{array}\right\} \tag{28}$$

To confirm the natural frequency and damping characteristics, a state-space representation of (21) is generated, $\dot{x}_E=A_Ex_E+B_Ed$, yielding the pair $\{A_E, B_E\}$:

$$A_E=\left[\begin{array}{cc:cc:cc} -2c/m & 1 & c/m & 0 & 0 & 0 \\ -2k/m & 0 & k/m & 0 & 0 & 0 \\ \hdashline c/(3m) & 0 & -2c/(3m) & 1 & c/(3m) & 0 \\ k/(3m) & 0 & -2k/(3m) & 0 & k/(3m) & 0 \\ \hdashline 0 & 0 & c/m & 0 & -2c/m & 1 \\ 0 & 0 & k/m & 0 & -2k/m & 0 \end{array}\right];\quad B_E=\left[\begin{array}{c} 0 \\ 0 \\ \hdashline 0 \\ 0 \\ \hdashline c/m \\ k/m \end{array}\right] \tag{29}$$

where:

$$x_E=\left[x_{E1}\quad x_{E2}\quad x_{E3}\quad x_{E4}\quad x_{E5}\quad x_{E6}\right]^T,\ \left[x_{E1}\quad x_{E3}\quad x_{E5}\right]=\left[y_{E1}\quad y_{E2}\quad y_{E3}\right]$$

$$\text{and}\ \left[\dot{x}_{E2}\quad \dot{x}_{E4}\quad \dot{x}_{E6}\right]=\left[\left(-\frac{2k}{m}y_{E1}+\frac{k}{m}y_{E2}\right)\ \left(\frac{k}{3m}y_{E1}-\frac{2k}{3m}y_{E2}+\frac{k}{3m}y_{E3}\right)\ \left(\frac{k}{m}y_{E2}-\frac{2k}{m}y_{E3}+\frac{k}{m}d\right)\right]$$

From A_E in (29), the numerical values for $\{m, k, c\}$ yield the natural frequencies, ω_n (and f_n in Hz), and the damping ratios, ζ, of Σ_E as:

$$\omega_n=\left[5.28\quad 14.1\quad 15.5\right]\text{rad/s}\ \Rightarrow\ f_n=\left[0.841\quad 2.25\quad 2.46\right]\text{Hz};\qquad \zeta=\left[0.00528\quad 0.0141\quad 0.0155\right]$$

7. ANALYSIS AND SYNTHESIS OF THE HYBRID SIMULATION SCHEME

This section introduces a simple first-order dynamic model for the actuator and the corresponding Σ_{HS} compensator design for the example of §6. Secondly, it provides an investigation of Σ_{HS} stability and robustness with respect to uncertainty in the actuator parameter, a, and at the same time considers the effect of three cases of split-mass ratio $R = m_2/m_1$, with a focus on the effect of this ratio upon stability. Thirdly, the effect of an actuator/transfer system pure delay term upon Σ_{HS} stability and robustness is investigated, again in conjunction with the three cases of mass ratio, R.

7.1 Actuator dynamics and Σ_{HS} compensator design.

Dynamic identification of a typical actuation system, for example a laboratory-based 25kN servohydraulic actuator, with its own discrete-time inner-loop displacement controller, yields an approximately first-order dynamic model for G_A; [14]. Hence, with reference to the notation of Figure 3:

$$G_A = \frac{y_2}{u} \approx \frac{\hat{a}}{s+\hat{a}}; \quad \hat{a} \approx 42.0\,\mathrm{s}^{-1} \tag{30}$$

where $\hat{a}$ is an estimate of a. From (6), the compensator design for Σ_{HS} is therefore given by:

$$G_C = \frac{u}{y_1} = \hat{G}_A^{-1} = \frac{s+\hat{a}}{\hat{a}} \approx \frac{s+42}{42(1+\varepsilon s)} \tag{31}$$

The denominator padding term, $(1+\varepsilon s)$, ensures properness of the compensator transfer function, G_C, whilst a very small value of ε does not cause a significant noise problem in this case, since the input signal to G_C is the numerically generated signal, y_1. If G_A is modelled as a higher order transfer function, with relative degree r, then it will be necessary to pad G_C with a term such as $(1+\varepsilon s)^r$.

7.2 Stability and robustness of Σ_{HS} with respect to a physical parameter change.

The robustness of Σ_{HS} is now investigated with respect to variations in the actuator parameter, a. For the present, the transfer system is assumed to contain no pure delay term; (see §7.3). Assuming that $\varepsilon \approx 0$, from (8), (26), (27) and (31) the CLCE of Σ_{HS} is:

$$1 - G_A G_C G_1 G_2 = 1 + \left(\frac{a}{s+a}\right)\left(\frac{s+\hat{a}}{\hat{a}}\right)\left(\frac{p_{21}}{p_{12}}\right) = 0 \tag{32}$$

Extracting a as the varying parameter, the CLCE can be written as:

$$1 + a\left[\frac{\hat{a}p_{12} + (s+\hat{a})p_{21}}{s\hat{a}p_{12}}\right] = 0 \quad \Rightarrow \quad 1 + KF = 0 \tag{33}$$

The term on the right of (33) is written in roots' loci canonical form, i.e. K is a linearly dependent parameter of a that increases monotonically along the loci paths and F is a monic transfer function. Hence, from the given value of $\hat{a}$:

$$K = \frac{am_2}{\hat{a}m_1} = \frac{a}{42}\left(\frac{m_2}{m_1}\right) = \frac{aR}{42} \tag{34}$$

Three cases of the split-mass ratio $R = (m_2/m_1)$ are considered in the following roots' loci analyses of Σ_{HS} robustness to changes in a: $R = \{0.5, 1.0, 2.0\}$. These are labelled as cases 1, 2 and 3, respectively, and in each case $m_1+m_2 = 3m = 300$ kg. From (26) and the given parameter data, $\{m, k, c\}$, the expressions for K and F in (33) are:

$$\left\{\begin{array}{ll}
\text{Case 1:} & K = 0.01191a; \quad F = \dfrac{s^5 + 126.6s^4 + 367.2s^3 + 33640s^2 + 13360s + 840000}{s(s^4 + 0.5000s^3 + 250.0s^2 + 20.00s + 5000)} \\
\text{Case 2:} & K = 0.02381a; \quad F = \dfrac{s^5 + 84.53s^4 + 311.5s^3 + 22430s^2 + 8907s + 560000}{s(s^4 + 0.5333s^3 + 266.7s^2 + 26.67s + 6667)} \\
\text{Case 3:} & K = 0.04762a; \quad F = \dfrac{s^5 + 63.50s^4 + 283.6s^3 + 16820s^2 + 6680s + 420000}{s(s^4 + 0.6000s^3 + 300.0s^2 + 40.00s + 10000)}
\end{array}\right\} \tag{35}$$

so that the corresponding CLCE roots' loci for each case are as shown in Figure 8.

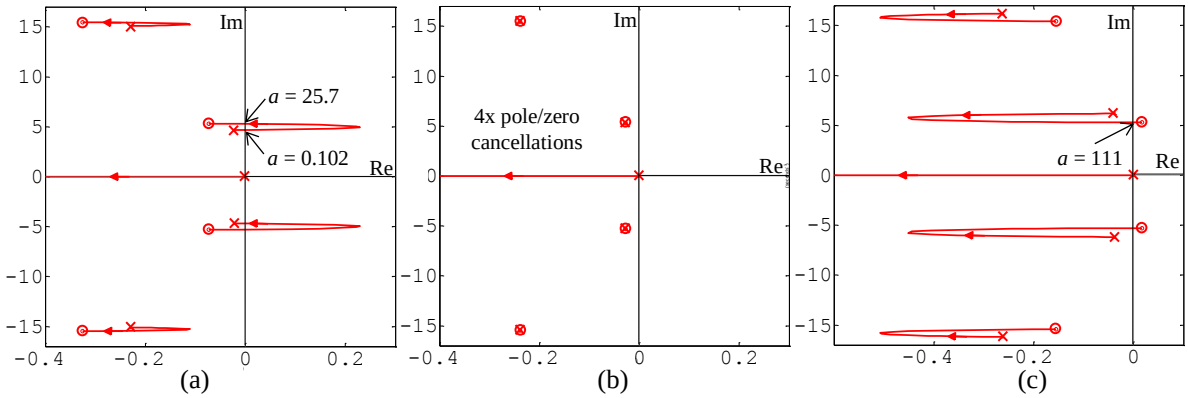

Fig. 8 Σ_{HS} roots' loci plots for a varying actuator constant, a.
(a) Case 1: $R = (m_2/m_1) = 0.5$ (b) Case 2: $R = (m_2/m_1) = 1.0$ (c) Case 3: $R = (m_2/m_1) = 2.0$

From Figure 8, it can be seen that (a) case 1 results in instability when $0.102 \leq a \leq 25.7$, (b) case 2 is unconditionally stable ($a > 0$) with four left-half plane pole/zero cancellations and (c) case 3 results in instability when $a \geq 111$. However, in all cases of a stable Σ_{HS}, poor relative stability will result since the dominant oscillatory roots are typically in the region of $-0.1 \pm 5j$, yielding a very small phase margin in the order of ~2°.

The purpose of the following simulations is to investigate the above stability analysis when the external disturbance, d, is a linear sinusoidal sweep signal of amplitude 3.0 mm and duration 200 s. The sweep starts at a frequency of 0.0 Hz and ends at a frequency of 4.0 Hz, thereby spanning the system natural frequencies. (In the following time plots, the frequency of excitation at a particular time t can therefore be determined as $f = t/50$ Hz). Figure 9 shows the resulting responses of Σ_E, $\{y_{E1}, y_{E2}, y_{E3}\}$, which remain constant throughout this work. When comparing results from stable system simulations, the difference between two signals will often be characterised in terms of performance indices defined as $I_{12} = [\int_0^{200} (y_1 - y_2)^2 dt]^{0.5}$ and $I_{E21} = [\int_0^{200} (y_{E2} - y_1)^2 dt]^{0.5}$, which are the indices of $\{\Sigma_1, \Sigma_2\}$-synchronisation and Σ_E-following (by Σ_1, at the substructure interface).

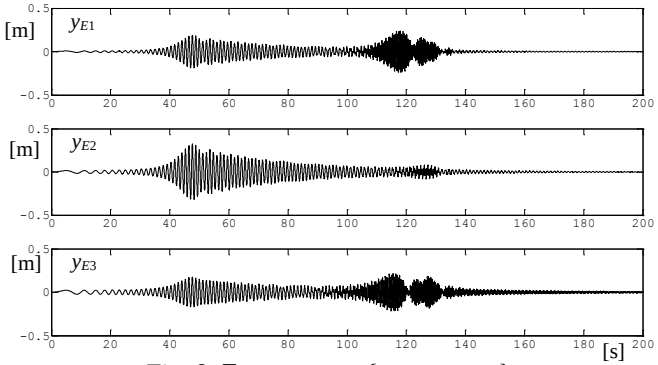

Fig. 9 Σ_E responses $\{y_{E1}, y_{E2}, y_{E3}\}$

For the present, no pure delay is assumed to exist in the dynamics of $\{\Sigma_1, \Sigma_2\}$. Delays have a significant effect upon stability and robustness results and this phenomenon is investigated in §7.3.

Case 1: $R = (m_2/m_1) = 0.5$; Σ_{HS} response.

As expected, the nominal value of the actuator parameter, $a = 42.0$ s^{-1}, results in stable and near-perfect responses with baseline performance indices of $I_{12} = 0.0$ mm.s and $I_{E21} = 1.8$ mm.s. Of more interest is the effect of a variation in the parameter to $a = 30.0$ s^{-1}, where Σ_{HS} is predicted to remain stable; the resulting responses of $\{\Sigma_1, \Sigma_2\}$ are presented in Figure 10(a). In particular, it is noted that the outputs $\{y_1, y_2\}$ have mediocre levels of synchronisation and Σ_E-following, with relatively large values for the performance indices of $I_{12} = 77.7$ mm.s and $I_{E21} = 798$ mm.s. Roots' loci analysis predicted instability when $0.102 \leq a \leq 25.7$. Thus, with $a = 25.0$ s^{-1}, the resulting unstable responses

of $\{\Sigma_1, \Sigma_2\}$ outputs are as shown in Figure 10(b); note that the synchronisation error, e, is also unstable. In fact, unstable responses exhibiting slow growth are generated up to the limits of the inequality $0.102 \leq a \leq 25.7$ (again, the results are not presented here).

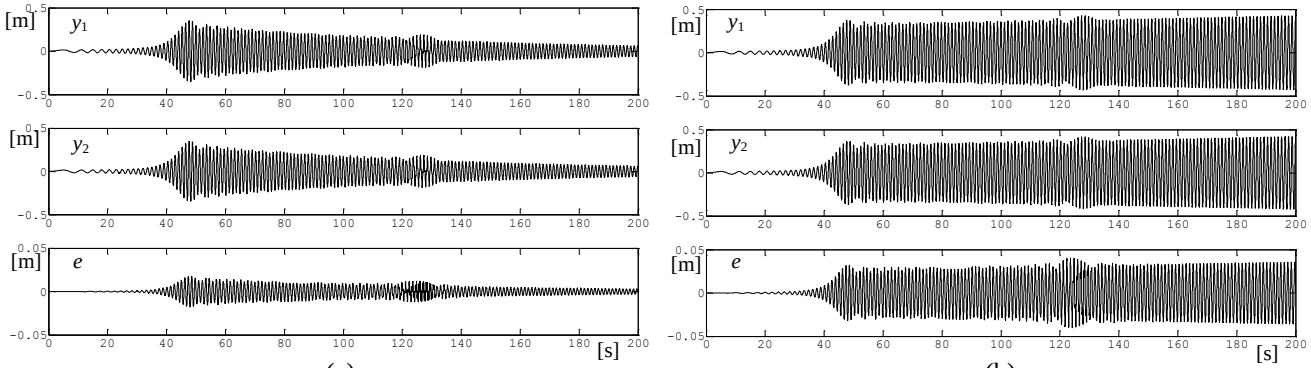

Fig. 10 Σ_{HS} case 1: $\{\Sigma_1, \Sigma_2\}$ responses $\{y_1, y_2\}$ and the error $e = y_1 - y_2$. (a) $a = 30$ s^{-1} (b) $a = 25$ s^{-1}

Case 2: $R = (m_2/m_1) = 1.0$; Σ_{HS} response.

This is the only case that guarantees unconditionally stable Σ_{HS} responses for $a > 0$, assuming that no pure delay is present. One set of results is presented. Retaining the parameter varied value of $a = 30.0$ s^{-1}, the corresponding response is shown in Figure 11. As predicted, the responses are stable, with improved performances compared with case 1: $I_{12} = 49.5$ mm.s and $I_{E21} = 24.7$ mm.s.

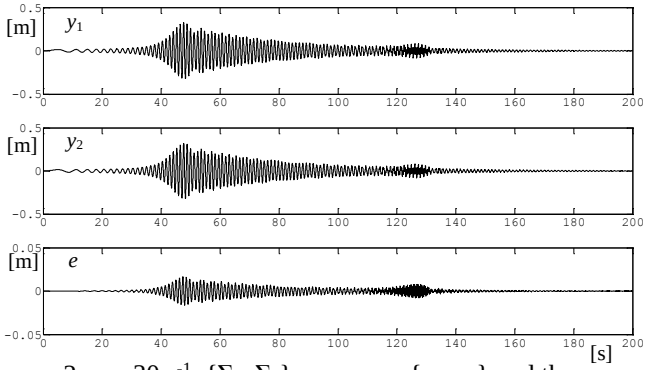

Fig. 11 Σ_{HS} case 2; $a = 30$ s^{-1}: $\{\Sigma_1, \Sigma_2\}$ responses $\{y_1, y_2\}$ and the error $e = y_1 - y_2$.

Case 3: $R = (m_2/m_1) = 2.0$; Σ_{HS} response.

Again, with the actuator parameter changed to $a = 30.0$ s^{-1}, Σ_{HS} is predicted to be stable. This is evident from Figure 12(a), where the response accuracy lies between those of case 1 and case 2; performance figures are $I_{12} = 39.6$ mm.s and $I_{E21} = 296$ mm.s. However, the roots' loci analysis does predict instability when $a \geq 111$ s^{-1}. Hence, setting $a = 130$ s^{-1}, for example, results in the unstable responses of Figure 12(b). Instability also occurs when $a = 111^+$ s^{-1} with an inevitably slow growth of the outputs; (these results are not presented here).

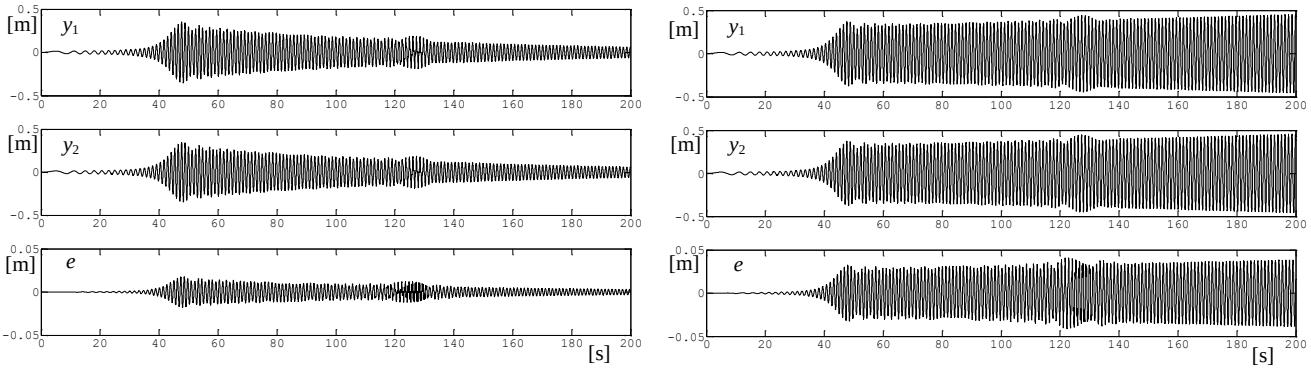

Fig. 12 Σ_{HS} case 3: $\{\Sigma_1, \Sigma_2\}$ responses $\{y_1, y_2\}$ and the error $e = y_1 - y_2$. (a) $a = 30$ s^{-1} (b) $a = 130$ s^{-1}

7.3 Stability and robustness of Σ_{HS} with respect to a pure delay term within the dynamics.

In addition to physical component parameter variations, the other phenomenon that can often beset substructured system control is a pure delay term within the dynamics. As described in §1, pure delays are most often the consequence of discrete-time computational elements within Σ_{TS}, or perhaps due to signal communication delays between geographically distant substructures. Therefore, Σ_{HS} is analysed in terms of its stability and robustness to the introduction of a pure delay term, $e^{-\tau s}$, within Σ_{TS}. Here, τ is the pure delay time, which is typically of the order of milliseconds. Due to the transcendental nature of the pure delay in the complex frequency domain, the algebraically rational roots' loci method (without modification) is no longer an appropriate approach to analysis. Therefore an alternative technique, based on classical Nyquist stability theory, is used to directly analyse the effect of pure delays.

Incorporating the pure delay in series with the compensator dynamics, G_C, (32) yields the revised Σ_{HS} CLCE as:

$$1-G_A(G_C e^{-\tau s})G_1G_2 = 1+\left(\frac{a}{s+a}\right)\left(\frac{s+\hat{a}}{\hat{a}}\right)\left(\frac{p_{21}}{p_{12}}\right)e^{-\tau s} = 0 \tag{36}$$

Assuming that the actuator parameter, a, is perfectly known for the purposes of this analysis, the CLCE in (36) becomes:

$$1+\underbrace{\left(\frac{p_{21}}{p_{12}}\right)e^{-\tau s}}_{H} = 1+H = 0 \tag{37}$$

and, according to Nyquist stability theory, the modulus and argument of open-loop transfer function, $H(j\omega)$, satisfy the following expressions at the point of closed-loop instability:

$$\left\{\begin{array}{l} \left|H(j\omega)\right| = \dfrac{\left|p_{21}(j\omega)\right|}{\left|p_{12}(j\omega)\right|} = 1 \\ \angle\{H(j\omega)\} = \angle\{p_{21}(j\omega)\} - \angle\{p_{12}(j\omega)\} - \omega\tau = -\pi \end{array}\right\} \tag{38}$$

Moreover, in the three-mass example, (p_{21}/p_{12}) has no poles or zeros in the right-half plane. Hence, the Nyquist right-hand rule (or 'Nyquist rule', for short) can be invoked: for the preservation of closed-loop stability, the polar plot of H must cross the negative real axis to the right of the critical point, -1+j0. In this work, the form of the polar plot of H at high frequencies is of crucial importance; from (26) and the left-hand side of (30), let $\omega \to \infty$:

$$\left|H\right\|_{\omega\to\infty} = \left.\frac{\left|p_{21}\right|}{\left|p_{12}\right|}\right|_{\omega\to\infty} = \frac{m_2}{m_1} = R; \quad \angle\{H\}\big|_{\omega\to\infty} = \left[\angle\{p_{21}\} - \angle\{p_{12}\} - \omega\tau\right]\Big\|_{\omega\to\infty} = -\omega\tau \tag{39}$$

i.e. at high frequencies the polar plot of H describes a circle of radius $R = (m_2 / m_1)$, centred on the origin of the complex plane. Hence, via the Nyquist rule, the following result is valid for all $\tau > 0$:

The HS scheme is unstable if the split-mass ratio $R = (m_2 / m_1) \geq 1$, i.e. if $m_2 \geq m_1$

Inevitably a pure delay, however small, will be present when discrete-time elements are used in the transfer system, so the above result places a significant and general restriction upon the applicability of the HS scheme when 'split-mass' substructured systems are to be tested. Although this is a sufficient, high-frequency condition for the existence of Σ_{HS} instability, it is not (by itself) necessary. The complete picture can be seen when re-investigating cases 1-3, whilst making use of the Nyquist rule over the entire frequency range of the polar plot.

Case 1: $R = (m_2/m_1) = 0.5$; Σ_{HS} polar plot.

The above condition for instability is not satisfied by the value of $R = 0.5$. However, analysis of the resulting polar plot leads to the conclusion that Σ_{HS} nevertheless will become unstable for values of τ exceeding a certain limit. Figure 13(a) shows the polar plot of H for this case. At very high frequencies, the curve describes the predicted circle of radius $R = (m_2 / m_1) = 0.5$, centred on the

origin. Via a trivial iterative procedure, the value of pure delay that ensures the negative real axis is tangential to the curve at the critical point, -1+*j*0, is found to be τ = 0.0147 s (at a frequency of ω = 5.28 rad/s). Increasing τ beyond this value will cause the polar plot to initially cross the real axis to the left of the critical point. Therefore the Nyquist rule predicts instability when $\tau \geq 0.0147$ s.

Case 2: $R = (m_2/m_1) = 1.0$; Σ_{HS} polar plot.

In this case, $p_{21} = p_{12}$, so that the only non-cancelled term within H is $e^{-j\omega\tau}$. Hence, when $\tau > 0$, the entire polar plot is a circle of radius $R = (m_2/m_1) = 1.0$, centred on the origin. Under these conditions Σ_{HS} will always be unstable according to the Nyquist rule.

Case 3: $R = (m_2/m_1) = 2.0$; Σ_{HS} polar plot.

Now the high frequency section of the polar plot has a radius $R = (m_2/m_1) = 2.0$, so again Σ_{HS} is always unstable when $\tau > 0$. The complete polar plot is shown in Figure 13(b), arbitrarily drawn for a pure delay time τ = 0.003 s.

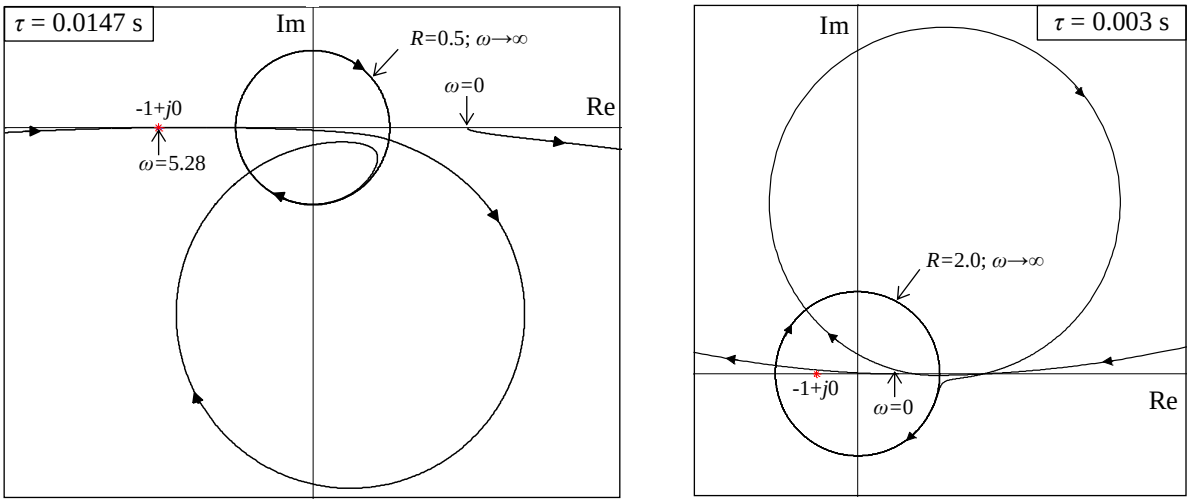

(a) (b)

Fig. 13 Σ_{HS} scheme polar plots of $H(j\omega)$ for varying mass ratio, R.
(a) Case 1: $R = (m_2/m_1) = 0.5$ (b) Case 3: $R = (m_2/m_1) = 2.0$

The following time-domain responses generated by the three cases, each with judicious selection of τ, provide additional insight into the problems associated with stability of Σ_{HS}.

Case 1: $R = (m_2/m_1) = 0.5$; Σ_{HS} response with pure delay.

This case exhibits conditional stability with increasing τ. Therefore when τ = 0.003 s, for example, a stable response is predicted by Figure 13(a) and the responses in Figure 14(a) bear this out. Synchronisation of $\{\Sigma_1, \Sigma_2\}$ outputs is acceptable, although Σ_E-following is less so, with performance measures of I_{12} = 17.6 mm.s and I_{E21} = 158 mm.s. However, instability is predicted if the delay is increased to τ = 0.016 s, for example, and Figure 14(b) shows the resulting responses.

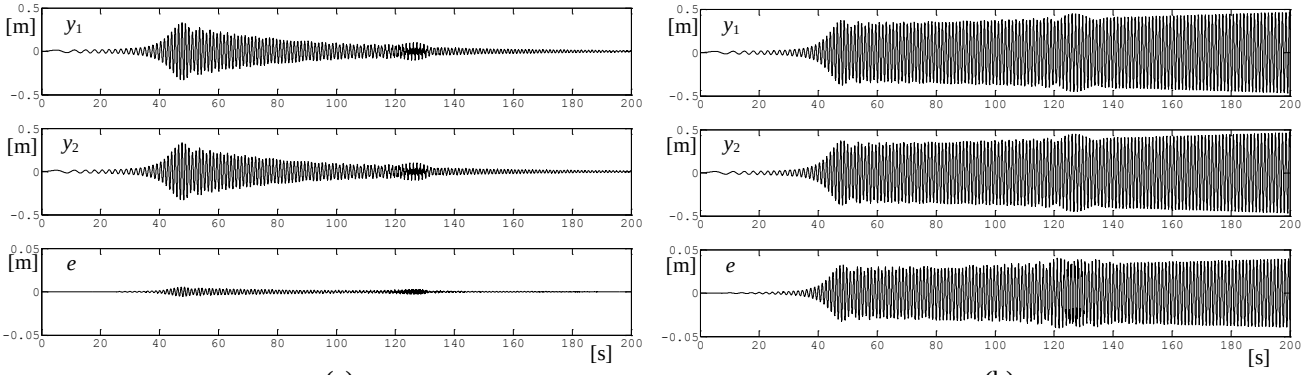

(a) (b)

Fig. 14 Σ_{HS} case 1: $\{\Sigma_1, \Sigma_2\}$ responses $\{y_1, y_2\}$ and the error $e = y_1 - y_2$. (a) τ = 0.003 s (b) τ = 0.016 s

Case 2: $R = (m_2/m_1) = 1.0$; Σ_{HS} response with pure delay.

This case is unstable for all $\tau > 0$, according to the Nyquist rule. For example, when $\tau = 0.003$ s the unstable response of Figure 15(a) is generated.

Case 3: $R = (m_2/m_1) = 2.0$; Σ_{HS} response with pure delay.

Again, this case is unstable for all $\tau > 0$ so that when $\tau = 0.003$ s, the unstable response of Figure 15(b) is the result.

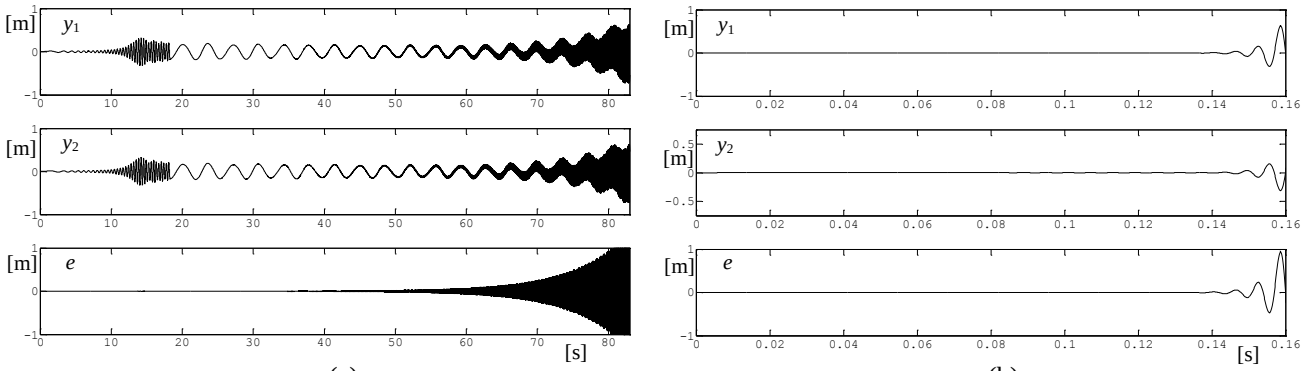

Fig. 15 Σ_{HS} ; $\tau = 0.003$ s: $\{\Sigma_1, \Sigma_2\}$ responses $\{y_1, y_2\}$ and the error $e = y_1 - y_2$.
(a) Case 2 (b) Case 3

8. ANALYSIS AND SYNTHESIS OF THE DYNAMICALLY SUBSTRUCTURED SYSTEM (DSS) SCHEME

This section introduces details of the DSS scheme when applied to the example of §6, in a similar manner to the approach taken with the HS scheme in §7.

8.1 Σ_{DSS} linear substructuring controller (LSC) design

The LSC has two components for design, K_d (= K_{d2}) and K_e, where the expression for K_d is determined using (12). From the expressions for the dynamics of $\{\Sigma_1, \Sigma_2\}$ and the actuator in (26), (27) and (30), after some manipulation (12) yields:

$$K_d = \frac{G_d G_1}{G_A(1-G_1G_2)} = \left(\frac{s+\hat{a}}{\hat{a}}\right)\left(\frac{(cs+k)^2}{p_{12}+p_{21}}\right) \tag{40}$$

which is of relative degree 1. The term $(p_{12}+p_{21}) = (ms^2+2cs+2k)(3ms^2+2cs+2k)-2(cs+k)^2$ in (40) is invariant for any mass ratio $R = m_2/m_1$, so that K_d is also invariant. Hence, the LSC forward transfer function is:

$$K_d = \frac{9.524s^3+9.924\times10^3 s^2+2.781\times10^6 s+10^8}{3.000\times10^4 s^4+1.600\times10^4 s^3+8.001\times10^6 s^2+8.000\times10^5 s+2\times10^8} \tag{41}$$

Also, the Σ_{DSS} CLECE is determined from (13) as:

$$1+G_A(1-G_1G_2)K_e = 1+\left(\frac{a}{s+a}\right)\underbrace{\left(\frac{p_{12}+p_{21}}{p_{12}}\right)}_{F_1}K_e = 1+\left(\frac{a}{s+a}\right)F_1K_e = 0 \tag{42}$$

so that the zeros of F_1 are invariant with the mass ratio, whereas the poles are not. Nevertheless, all poles and zeros of F_1 will be in the left-half s-plane, so the following stable pole/zero cancellation design is proposed for the LSC feedback transfer function, K_e:

$$K_e = F_1^{-1}\left(k_p+\frac{k_i}{s}\right) = k_pF_1^{-1}\left(\frac{s+k_i/k_p}{s}\right) \tag{43}$$

where k_p and k_i are proportional and integral gains, yet to be determined. Selecting the gain ratio $k_i / k_p = \hat{a}$, the CLECE in (42) is then independent of the mass ratio and can be written as:

$$1+\left(\frac{a}{s+a}\right)F_1K_e = 1+k_p\left(\frac{a}{s+a}\right)\left(\frac{s+\hat{a}}{s}\right)=0 \tag{44}$$

Assuming for the purposes of design that $a=\hat{a}=42$, (44) reduces to the first-order CLECE:

$$s+42k_p=0 \tag{45}$$

so that setting k_p = 1, (and hence k_i = 42), yields a CL error transient settling-time of ~0.1 s.

8.2 Stability and robustness of Σ_{DSS} with respect to a physical parameter change.

The feedback component of the LSC design, characterised by the CLECE in (44), is examined for its effect on stability and robustness to changes in the key actuator parameter, a. Therefore, assigning a as the parameter of variation, (44) can be re-written in roots' loci canonical form as:

$$1+a\left(1+k_p\right)\left[\frac{s+\left(\hat{a}k_p\right)/\left(1+k_p\right)}{s^2}\right]=1+\underset{K}{2a}\underbrace{\left[\frac{s+21}{s^2}\right]}_{F}=0 \tag{46}$$

The resulting roots' loci are shown in Figure 16, indicating that the Σ_{DSS}-LSC strategy is unconditionally stable for all $a > 0$, (and for all cases of mass ratio), which is in sharp contrast to the stability and robustness results for the Σ_{HS} scheme shown in Figure 8.

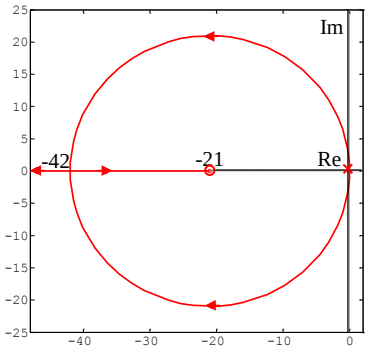

Fig. 16 Σ_{DSS} scheme roots' loci for a varying actuator constant, a; valid for all mass ratios.

Σ_{DSS} responses are compared with those of Σ_{HS}, for the values of mass ratio, R, and actuator parameter, a, previously used. As in §7.2, there are no pure delay terms yet included within the substructure dynamics (see §8.3 for detailed comments on the issue of Σ_{DSS} with pure delays).

Case 1: $R = (m_2/m_1) = 0.5$; Σ_{DSS} response.

Figure 17(a) shows the Σ_{DSS} responses when the actuator parameter value is varied from the nominal value to a = 30 s^{-1}. Comparing this with the equivalent Σ_{HS} responses in Figure 10(a), the synchronisation error, e, of Σ_{DSS} is seen to be of a consistently smaller amplitude than that of Σ_{HS}, yielding I_{12} = 12.5 mm.s, a factor of ~6.2 improvement. In addition, the responses of $\{\Sigma_1, \Sigma_2\}$, y_1 and y_2, generated by Σ_{DSS} are now much closer to the desired emulated response, y_{E2}, shown in Figure 9. The associated I_{E21} = 12.1 mm.s represents a ~66 improvement over the Σ_{HS} result. Decreasing the actuator parameter to a = 25 s^{-1} results in instability of Σ_{HS}, but as predicted Σ_{DSS} remains stable. See Figure 17(b), which illustrates the excellent $\{\Sigma_1, \Sigma_2\}$ synchronisation and correspondence with the emulated response, y_{E2}, yielding I_{12} = 21.4 mm.s and I_{E21} = 21.2 mm.s.

Note: Due to the efficacy of control, subsequent Σ_{DSS} and Σ_{USS} responses closely match those in Figure 17 and will not be presented here. However, the resulting performance indices are presented and also included in the comparative Table 1 at the end of this section.

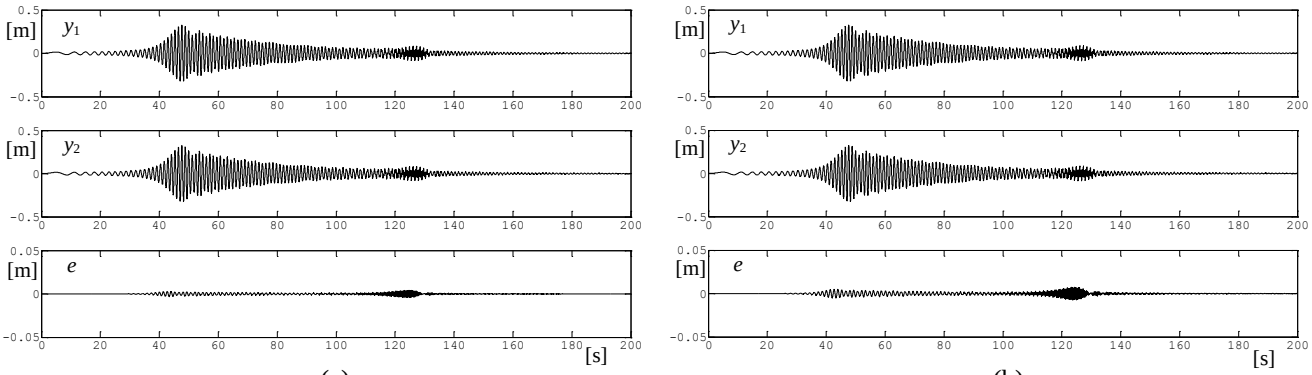

Fig. 17 Σ_{DSS} case 1: $\{\Sigma_1, \Sigma_2\}$ responses $\{y_1, y_2\}$ and the error $e = y_1 - y_2$. (a) $a = 30$ s^{-1} (b) $a = 25$ s^{-1}

Case 2: $R = (m_2/m_1) = 1.0$; Σ_{DSS} response.

This is the only case that ensures unconditional stability of Σ_{HS} (with no pure delay present). Setting $a = 30$ s^{-1}, the resulting Σ_{HS} response of Figure 11 yields $I_{12} = 49.5$ mm.s and $I_{E21} = 24.7$ mm.s, which are significantly outperformed by the corresponding Σ_{DSS}, with indices $I_{12} = 16.2$ mm.s and $I_{E21} = 9.81$ mm.s.

Case 3: $R = (m_2/m_1) = 2.0$; Σ_{DSS} response.

With $a = 30$ s^{-1}, Σ_{HS} is shown to be stable in Figure 12(a), yielding $I_{12} = 39.6$ mm.s and $I_{E21} = 296$ mm.s. The equivalent Σ_{DSS} again yields a superior performance, with $I_{12} = 22.8$ mm.s and $I_{E21} = 22.7$ mm.s. Increasing the parameter value to $a = 30$ s^{-1} yields an unstable Σ_{HS} response (see Figure 12(b)), whereas the equivalent Σ_{DSS} response remains stable. The resulting Σ_{DSS} performance indices are $I_{12} = 36.3$ mm.s and $I_{E21} = 37.7$ mm.s.

8.3 Stability and robustness of Σ_{DSS} with respect to a pure delay term within the dynamics

In a similar manner to the development in §7.3, the Nyquist rule is applied to the polar plot of the open-loop transfer function, H, of Σ_{DSS} when there is a pure delay term, $e^{-\tau s}$, in the actuator transfer function, G_A. Using the LSC design from §8.2 and assuming that the actuator parameter is known exactly, i.e. $\hat{a} = a$, from (44) the CLCE is given by:

$$\underbrace{1 + k_p \left(\frac{a}{s} \right) e^{-\tau s}}_{H} = 0 \tag{47}$$

Hence, H satisfies the following conditions for the onset of closed-loop instability:

$$\left| H(j\omega) \right| = \frac{a k_p}{\omega} = 1 \;\Rightarrow\; \omega_c = a k_p ; \qquad \angle \left\{ H(j\omega) \right\} = -\frac{\pi}{2} - \omega\tau = -\pi \;\Rightarrow\; \tau_c = \frac{\pi}{2\omega_c} \tag{48}$$

where ω_c and τ_c are the values of the frequency and pure delay at the critical point, -1+j0. From §8.2, $k_p = 1$, so that $\omega_c = 42$ rad/s and $\tau_c = 0.0374$ s. Note that this result is independent of the mass ratio, R, and that the limit on the pure delay is significantly higher than for Σ_{HS}. The corresponding polar plot is shown in Figure 18, when $\tau = 0.0374$ s.

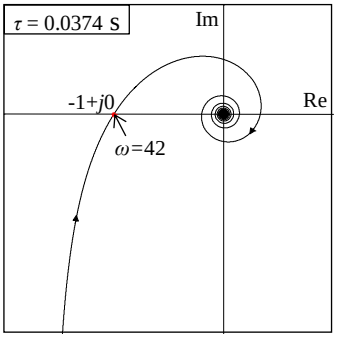

Fig. 18 Σ_{DSS} scheme polar plot of $H(j\omega)$.

For case 1 of the mass ratio, the resulting Σ_{DSS} responses are examined for the pure delays $\tau = 0.003$ s and $\tau = 0.016$ s. When $\tau = 0.003$ s, the performance indices are $I_{12} = 3.99$ mm.s and $I_{E21} = 3.81$ mm.s, which compare favourably with the equivalent results from Σ_{HS}, (Figure 14(a)), where $I_{12} = 17.6$ mm.s and $I_{E21} = 158$ mm.s. However, with an increase in pure delay to $\tau = 0.016$ s Σ_{HS} is unstable, (Figure 14(b)), but as expected Σ_{DSS} remains stable with performance indices $I_{12} = 22.1$ mm.s and $I_{E21} = 21.5$ mm.s.

The pure delay is now fixed at $\tau = 0.003$ s and the Σ_{DSS} responses are compared with those of Σ_{HS} for the mass-ratio cases 2 and 3. In both cases Σ_{HS} is shown to be unstable; see Figure 15. However, as predicted Σ_{DSS} remains stable with case 2 performance indices of $I_{12} = 5.27$ mm.s and $I_{E21} = 4.70$ mm.s, whilst for case 3 the indices are $I_{12} = 7.44$ mm.s and $I_{E21} = 7.69$ mm.s.

The two retrofit Σ_{USS} strategies are examined for the mass-ratio of case 3 and a pure delay time $\tau = 0.003$ s, in order to compare the responses with those of the equivalent Σ_{DSS}. The resulting nearly-exact correspondence is borne out by the performance indices: again, for Σ_{DSS} $I_{12} = 7.44$ mm.s and $I_{E21} = 7.69$ mm.s; for the Σ_{USS} pre-Σ_{HS} retrofit $I_{12} = 7.44$ mm.s and $I_{E21} = 7.69$ mm.s; for the Σ_{USS} post-Σ_{HS} retrofit $I_{12} = 7.41$ mm.s and $I_{E21} = 7.80$ mm.s. Based on these results, the Σ_{USS} pre-Σ_{HS} retrofit strategy has performed exactly the same as Σ_{DSS}. There is a marginal difference between the Σ_{USS} post-Σ_{HS} retrofit strategy and Σ_{DSS}, which can be explained by the padding required within the denominator of K_{ec}.

Finally, Table 1 summarises the performance indices for all stable simulations conducted in §§7, 8, from which the relative effectiveness of Σ_{HS} can be compared with Σ_{DSS} and Σ_{USS}.

Test Conditions (Italics indicate nominal parameters. Unlisted parameters are also nominal)			**Performance Indices**			
			Σ_{HS}		Σ_{DSS} (Σ_{USS})	
Case	a [s^{-1}]	τ [ms]	I_{12} [mm.s]	I_{E21} [mm.s]	I_{12} [mm.s]	I_{E21} [mm.s]
1	*42*	*0*	0.0	1.8	0.0	1.8
1	30	*0*	77.7	798	12.5	12.1
1	25	*0*	Unstable		21.4	21.2
2	30	*0*	49.5	24.7	16.2	9.81
3	30	*0*	39.6	296	22.8	22.7
3	130	*0*	Unstable		36.3	37.7
1	*42*	3	17.6	159	3.99	3.81
1	*42*	16	Unstable		22.1	21.5
2	*42*	3	Unstable		5.27	4.70
3	*42*	3	Unstable		7.44	7.69
3	*42*	3			(7.44)	(7.69)
3	*42*	3			(7.41)	(7.80)

Table 1 Performance indices I_{12} and I_{E21} for all stable tests.

9. CONCLUSION AND DISCUSSION

The main conclusions to be drawn from this work are as follows:

(1) The essential elements of a substructured testing system are a numerical substructure (Σ_1), a physical substructure (Σ_2) and a transfer system (Σ_{TS}), where the latter links $\{\Sigma_1, \Sigma_2\}$ together at their interface, all within a closed-loop configuration. In turn, Σ_{TS} consists of an actuator and a compensator/controller. The purpose of the compensator/controller is to ensure satisfaction of the principal objective for a substructured testing system (see (2)).

(2) The *principle objective* is to ensure that the substructured system dynamics and its responses closely match those of a pre-defined emulated system, Σ_E. More specifically, the requirement

at the substructure interface is for close synchronisation and Σ_E-following of the $\{\Sigma_1, \Sigma_2\}$ outputs. In addition, this should be achieved despite the presence of any physical parameter uncertainties and pure delays in signal transmissions.

(3) Parameter uncertainty will usually occur within the dynamics of the actuator and Σ_2. Pure delays will usually occur within Σ_{TS}, and specifically within the actuator's inner-loop controller, which is usually a discrete-time device.

(4) With reference to the last comment in (1), the hybrid simulation (Σ_{HS}) scheme is frequently used for the design of an *inverting compensator* in Σ_{TS}, whereas the dynamically substructured system (Σ_{DSS}) scheme is used for the design of an *automatic controller*.

(5) It has been shown that Σ_{HS} and Σ_{DSS} can share a *common framework* for analysis and synthesis of substructured systems.

(6) The structure of Σ_{HS} admits an intuitively simple design for the compensator. Hence, use of the common framework enables Σ_{DSS} and its associated linear substructuring controller (LSC) to be synthesised in a more intuitive manner than has been hitherto possible using the original techniques described in [1].

(7) Classical control techniques are effective tools for the analysis of Σ_{HS} or Σ_{DSS} and the synthesis of the associated compensator/controller.

(8) It was shown that the Σ_{HS} formulation can achieve excellent results under conditions of parameter certainty and no pure delays in the system. Otherwise, stability and robustness of the method were degraded significantly, to the point of crossing the boundary of instability. This is especially so with lightly damped Σ_{HS}, such as structural systems.

(9) Conversely, the Σ_{DSS} formulation possesses significantly improved levels of relative stability and robustness, so that it can satisfy the principle objective under conditions of parameter uncertainty and pure delays present in the system.

(10) The fundamental reasons for the conclusions in (8) and (9) are as follows. Firstly, Σ_E and Σ_{HS} have identical closed-loop characteristic equations (CLCE), so that lightly-damped characteristics of Σ_E automatically appear as poor relative stability and robustness characteristics in Σ_{HS}. Secondly, although Σ_{DSS} and Σ_E also have an identical CLCE, the closed-loop *error* dynamics of Σ_{DSS} can be configured separately to have arbitrary (finite) levels of relative stability and robustness, via a suitable design of the LSC.

(11) The common framework enables a unified substructured system (Σ_{USS}) retrofit strategy, whereby a Σ_{DSS}-synthesised control loop can be added to an existing Σ_{HS} implementation in order to improve synchronisation accuracy, stability and robustness.

(12) A simulation example was presented to illustrate and support the above comments and assertions. In particular, the example was configured to show the effects of the substructured interface occurring within an inertial element (the split-mass problem), physical parameter uncertainty and the presence of a pure delay in Σ_{TS}.

(13) This investigation has been primarily concerned with linear dynamical systems. However the use of an adaptive control algorithm, specifically tailored to the DSS framework, can significantly improve robustness to parameter uncertainty and the presence of non-linear dynamics (such as hardening/softening behaviour in compliant elements); [1], [14], [15].

(14) To summarise: the principle advantages of DSS over HS are significantly improvements in stability margins, robustness to parameter uncertainties and accuracy of responses. The main disadvantage is the additional design effort that is required. USS retains the advantages of DSS, with the additional advantage that the commonly-used HS strategy can be retained within the test system.

A brief discussion on the results generated by the simulated example now follows. The general observation has been that Σ_{DSS} consistently outperforms Σ_{HS} in terms of $\{\Sigma_1, \Sigma_2\}$ synchronisation

and Σ_E-following. To quantify this observation over the set of all stable Σ_{HS} and Σ_{DSS} simulations, *S*, the mean time responses of the synchronisation index, $\tilde{I}_{12} = \underset{S}{\text{mean}}\left[\int_0^t (y_1 - y_2)^2 dt\right]^{1/2}$, and the Σ_E-following index, $\tilde{I}_{E21} = \underset{S}{\text{mean}}\left[\int_0^t (y_{E2} - y_1)^2 dt\right]^{1/2}$, are shown in Figure 19. It is evident that performance improvements of Σ_{DSS} over Σ_{HS}, as measured at the end of the simulations, are ~2.8-fold in terms of $\{\Sigma_1, \Sigma_2\}$ synchronisation and ~20-fold in terms of Σ_E-following. Furthermore, the consistency-ratio between the two indices, defined as $\tilde{I}_{E21} : \tilde{I}_{12}$ at the end-times, are ~0.95 for Σ_{DSS} and ~6.9 for Σ_{HS}. The implication is that Σ_{DSS} is remarkably consistent at satisfying both aspects of the principle objective, whilst Σ_{HS} is particularly poor at the task of Σ_E-following.

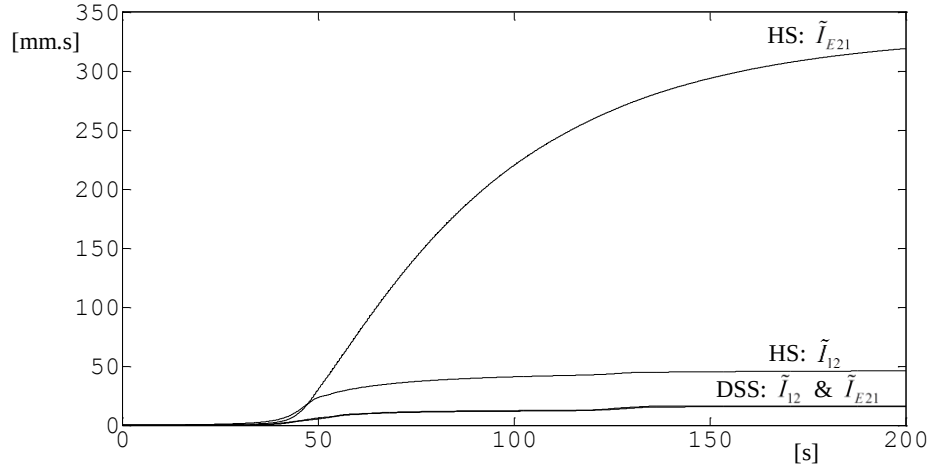

Fig. 19 Mean performance index time-trajectories for the Σ_{HS} and Σ_{DSS} schemes

ACKNOWLEDGEMENT

The author would like to thank Dr Ryuuta Enokida, Japan Society for the Promotion of Science Research Fellow in the ACTLab, University of Bristol, for his advice on the history, development and use of the hybrid simulation scheme.

ABBREVIATIONS

	General:
CE	Characteristic equation
CL	Closed-loop
CLCE	Closed-loop characteristic equation
CLECE	Closed-loop error characteristic equation
CP	Characteristic polynomial
DOF	Degree of freedom
DSS	Dynamically substructured system; (Σ_{DSS})
HiLS	Hardware-in-(the)-loop simulation
HS	Hybrid simulation (system); (Σ_{HS})
LSC	Linear substructured (system) controller
PID	Proportional-integral-derivative (controller)
TS	Transfer system; (Σ_{TS})
USS	Unified substructured system; (Σ_{USS})
	Systems (Σ):
Σ_1	(Numerical) substructure
Σ_2	(Physical) substructure
Σ_{DSS}	Dynamically substructured system
Σ_E	Emulated system
Σ_{HS}	Hybrid simulation system
Σ_{TS}	Transfer system
Σ_{USS}	Unified substructured system

REFERENCES

1. Stoten DP, Hyde RA. Adaptive control of dynamically substructured systems: the single-input single-output case. *Proc. IMechE, Part I: J. Systems and Control Engineering*, 2006, **220**(2):63-79.
2. Nakashima M, Kato H, Takaoka E. Development of real-time pseudo dynamic testing. *Earthquake Engineering and Structural Dynamics*, 1992, **21**(1):79-92.
3. Horiuchi T, Inoue M, Konno T, Namita Y. Real-time hybrid experimental system with actuator delay compensation and its application to a piping system with an energy absorber. *Earthquake Engineering and Structural Dynamics*, 1999, **28**(10):1121-1141.
4. Magonette G. Development and application of large-scale continuous pseudo-dynamic testing techniques. *Phil. Trans. R. Soc. Lond.* A, 2001, **359**(1786):1771-1799.

5. Brandt EP, Wang Y, Grizzle JW. A simplified three-way catalyst model for use in on-board SI engine control and diagnostics. *Proc. ASME Dynamic Systems and Control*, 1997:653-659.
6. Raman S, Sivashankar N, Milam W, Stuart W, Nabi S. Design and implementation of HiL simulators for powertrain control system software development. *Proc. American Control Conference*, San Diego, CA, June 1999:709-713.
7. Darby AP, Blakeborough A, Williams MS. Real-time substructure tests using hydraulic actuators, *J. Eng. Mech.*, 1999, **125**(10):1133–1139.
8. Horiuchi T, Konno T. A new method for compensating actuator delay in real-time hybrid experiments, *Phil. Trans. R. Soc. Lond.* A, 2001, **359**(1786):1893–1909.
9. Ahmadizadeh M, Mosqueda G, Reinhorn AM. Compensation of actuator delay and dynamics for real-time hybrid structural simulation, *Earthquake Engineering and Structural Dynamics*, 2008, **37**(1):21–42.
10. Carrion J, Spencer B. Model-based strategies for real-time hybrid testing, *NSEL report* NSEL-006, 2007, University of Illinois at Urbana-Champaign.
11. Chen C, Ricles JM. Improving the inverse compensation method for real-time hybrid simulation through a dual compensation scheme, *Earthquake Engineering and Structural Dynamics*, 2009, **38**(10):1237–1255.
12. Philips MB, Spencer B. Model-based feedforward-feedback actuator control for real-time hybrid simulation, *J. Struct. Eng.*, 2013, **139**(7):1205–1214.
13. Stoten DP. A comparison of hybrid and DSS schemes for substructured system testing, *Proceedings of MOVIC 2014 - 12th Int. Conf. Motion and Vibration Control*, Japan Society of Mechanical Engineers, Sapporo, Japan, August 2014.
14. Stoten DP, Tu J-Y, Li G. Synthesis and control of generalised dynamically substructured systems, *Proc. IMechE, Part I: J. Systems and Control Engineering*, 2009, **223**:371-392.
15. Tu J-Y, Lin P-Y, Stoten DP, Li G. Testing of dynamically substructured, base-isolated systems using adaptive control techniques, *Earthquake Engineering and Structural Dynamics*, 2010, **39**(6):661-681.
16. Enokida R, Stoten DP, Kajiwara K. Stability analysis and comparative experimentation for two substructuring schemes, with a pure time delay in the actuation system. *Journal of Sound and Vibration*, 2015, **346**:1-16.
17. Tu J-Y, Stoten DP, Li G, Hyde RA. A state-space approach for the control of multivariable dynamically substructured systems, *Proc. IMechE, Part I: J. Systems and Control Engineering*, 2011, **225**:935-953.
18. Wu B, Deng L, Yang X. Stability of central difference method for dynamic real-time substructure testing. *Earthquake Engineering and Structural Dynamics*, 2009, **38**:1649–1663.
19. Gawthrop PJ, Neild SA, Gonzalez-Buelga A, Wagg DJ. Causality in real-time dynamic substructure testing. *Mechatronics*, 2009, **19**(7):1105-1115.
20. Wang Z, Bursi OS, Wu B. Equivalent force control method with acceleration correction for real-time substructure testing of a split-mass system, *11th Int. Symp. Structural Engineering*, Guangzhou, China, December 2010:00-06.
21. Wu B, Wang Z, Bursi OS. Actuator dynamics compensation based on upper bound delay for real-time hybrid simulation. *Earthquake Engineering and Structural Dynamics*, 2013, **42(**12): 1749-1765.
22. D'Azzo JJ, Houpis CH. *Feedback Control System Analysis and Synthesis*, 1966, Kougakusha Co. Ltd, Tokyo.

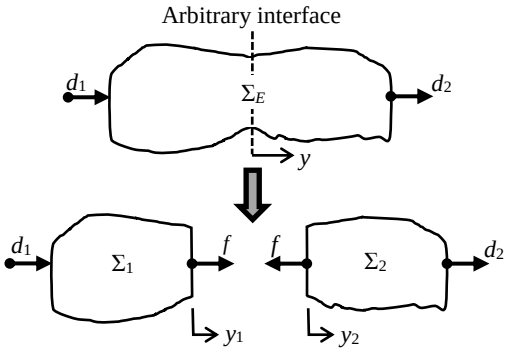

Fig. 1 A generalised emulated system, Σ_E, and its associated substructured systems, $\{\Sigma_1, \Sigma_2\}$.

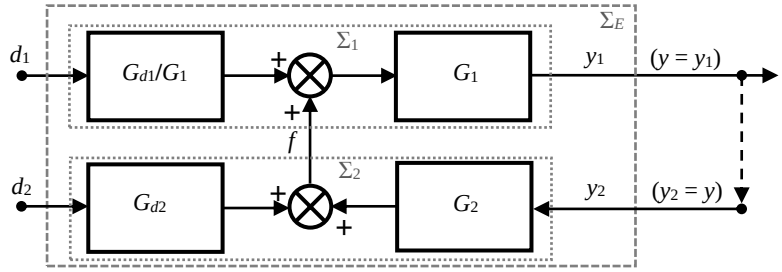

Fig. 2 Σ_E showing the $\{\Sigma_1, \Sigma_2\}$ components in a quasi closed-loop form.

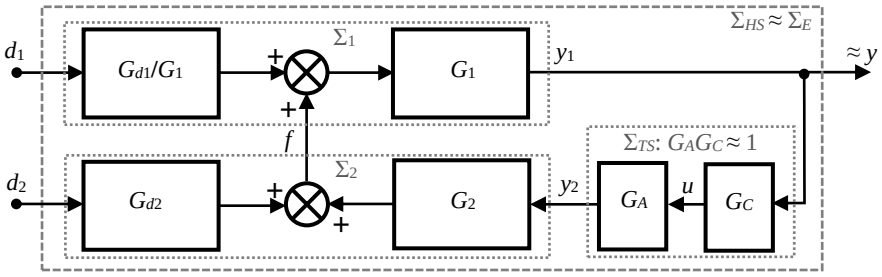

Fig. 3 Σ_{HS} in closed-loop form with an actuator, G_A, and compensator, G_C.

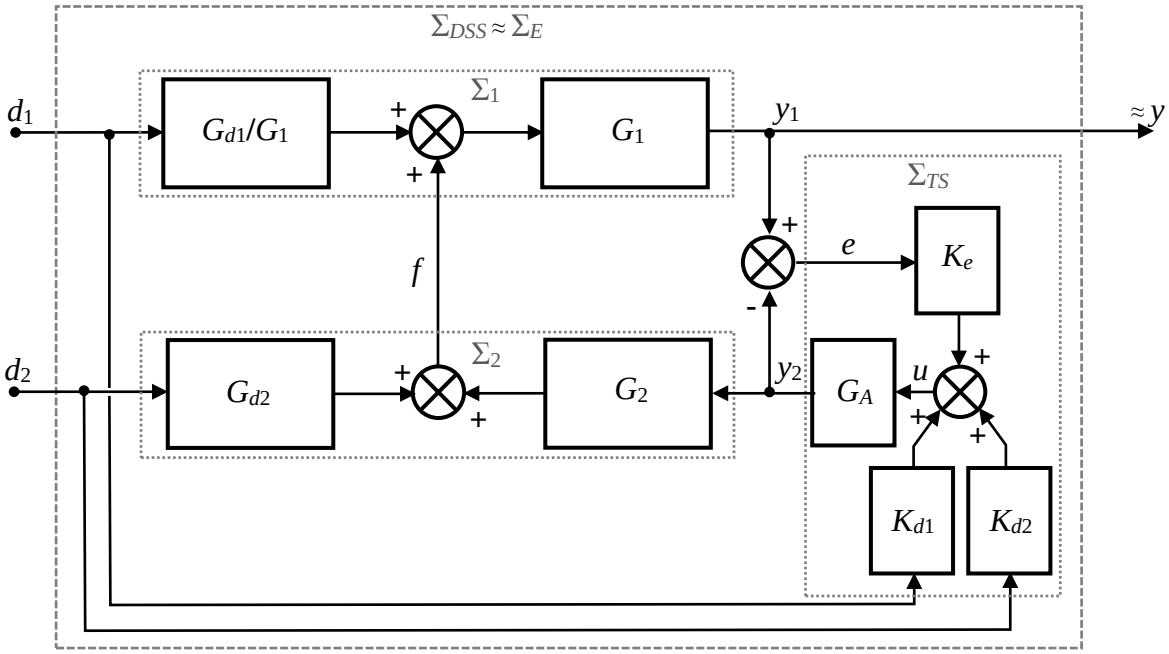

Fig. 4 Σ_{DSS} based upon the amalgamation of the Σ_{HS} formulation of Figure 3 and reference [1].

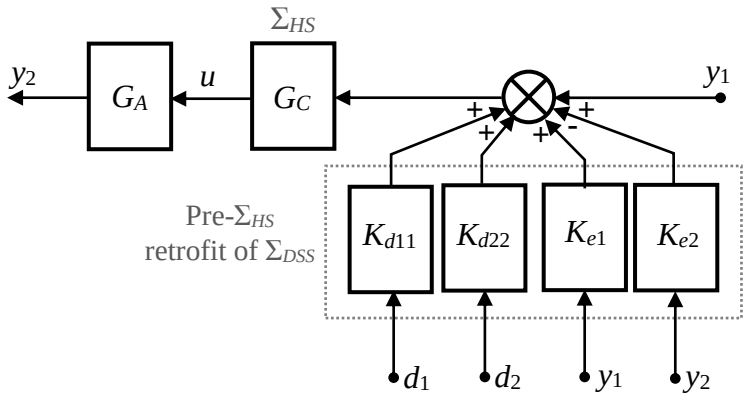

Fig. 5 Σ_{USS}: pre-Σ_{HS} retrofit of Σ_{DSS}.

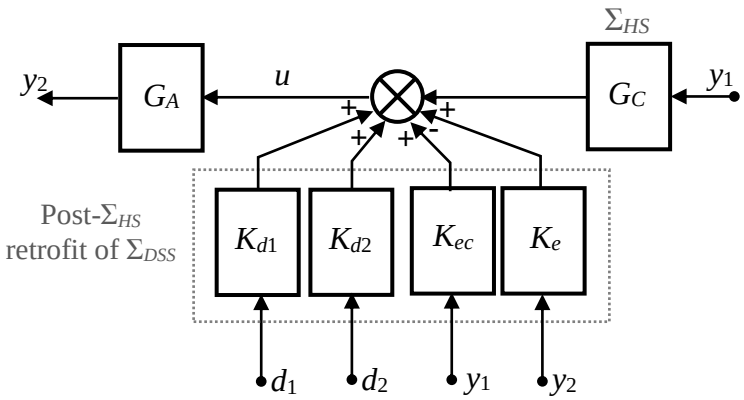

Fig. 6 Σ_{USS}: post-Σ_{HS} retrofit of Σ_{DSS}.

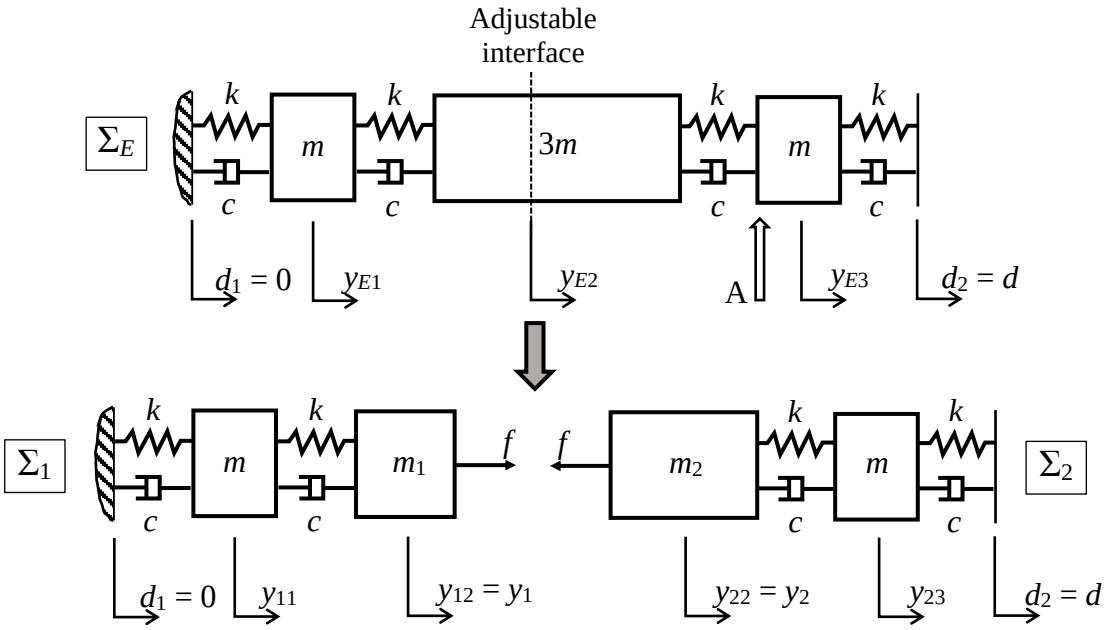

Fig. 7 The emulated system, Σ_E (top) and the 2 substructures $\{\Sigma_1, \Sigma_2\}$ (bottom); Σ_1 is the numerical substructure and Σ_2 is the physical substructure.

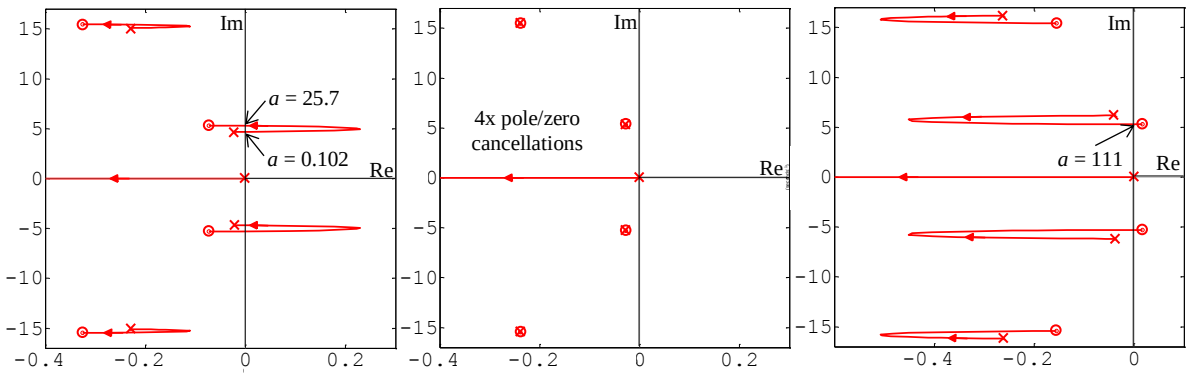

Fig. 8 Σ_{HS} roots' loci plots for a varying actuator constant, a.
(a) Case 1: $R = (m_2/m_1) = 0.5$ (b) Case 2: $R = (m_2/m_1) = 1.0$ (c) Case 3: $R = (m_2/m_1) = 2.0$

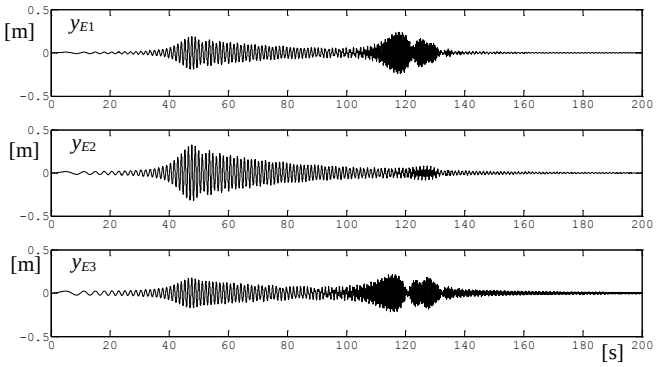

Fig. 9 Σ_E responses $\{y_{E1}, y_{E2}, y_{E3}\}$

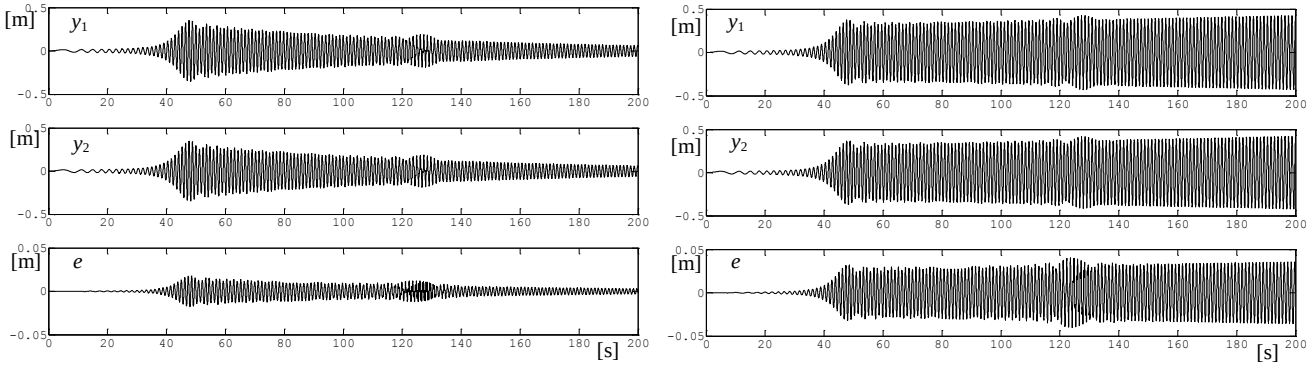

(a) (b)

Fig. 10 Σ_{HS} case 1: $\{\Sigma_1, \Sigma_2\}$ responses $\{y_1, y_2\}$ and the error $e = y_1 - y_2$. (a) $a = 30\ s^{-1}$ (b) $a = 25\ s^{-1}$

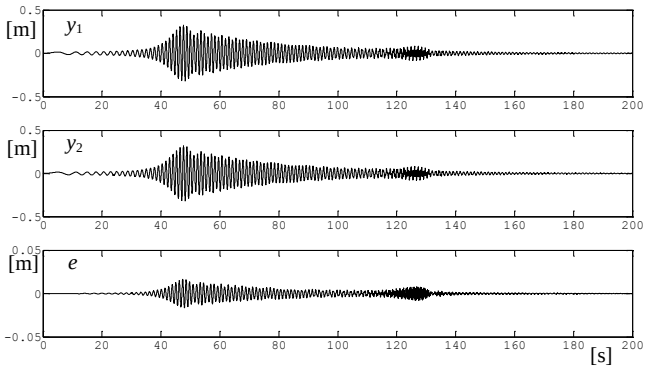

Fig. 11 Σ_{HS} case 2; a = 30 s^{-1}: $\{\Sigma_1, \Sigma_2\}$ responses $\{y_1, y_2\}$ and the error $e = y_1 - y_2$.

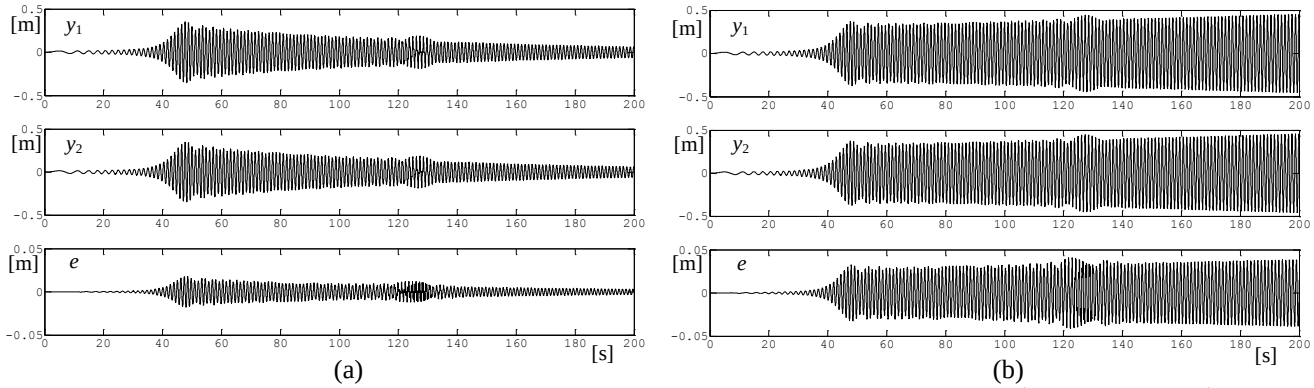

Fig. 12 Σ_{HS} case 3: $\{\Sigma_1, \Sigma_2\}$ responses $\{y_1, y_2\}$ and the error $e = y_1 - y_2$. (a) $a = 30$ s^{-1} (b) $a = 130$ s^{-1}

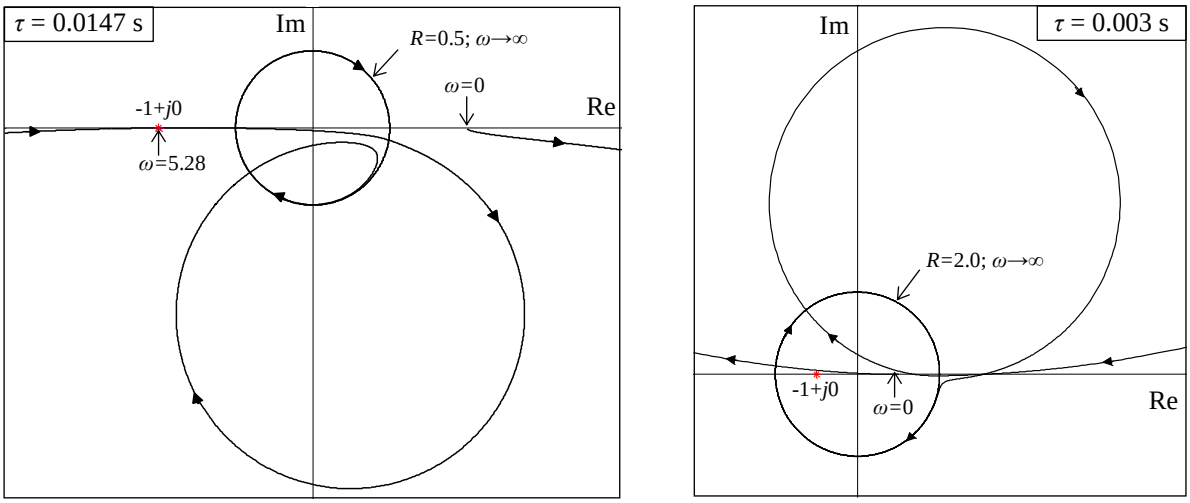

(a) (b)

Fig. 13 Σ_{HS} scheme polar plots of $H(j\omega)$ for varying mass ratio, R.
(a) Case 1: $R = (m_2/m_1) = 0.5$ (b) Case 3: $R = (m_2/m_1) = 2.0$

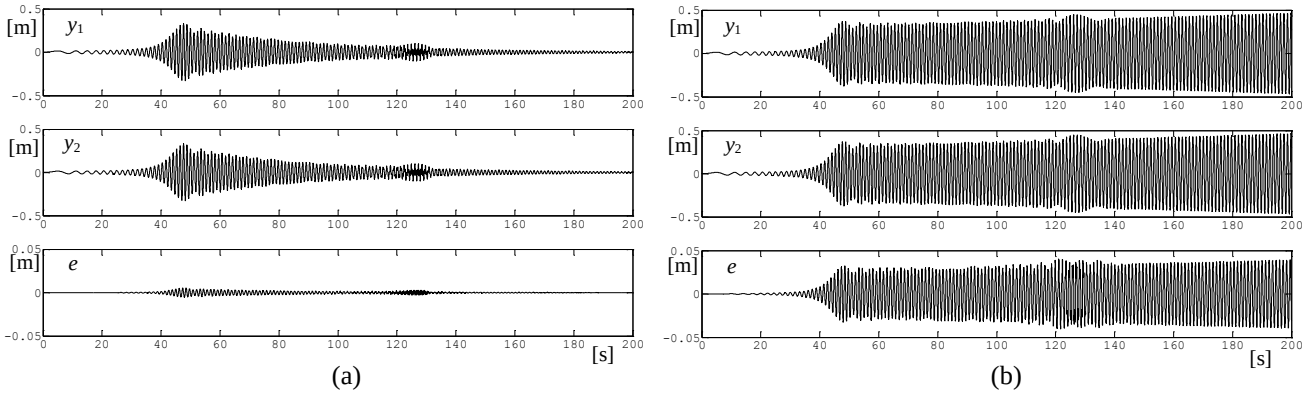

Fig. 14 Σ_{HS} case 1: $\{\Sigma_1, \Sigma_2\}$ responses $\{y_1, y_2\}$ and the error $e = y_1 - y_2$. (a) $\tau = 0.003$ s (b) $\tau = 0.016$ s

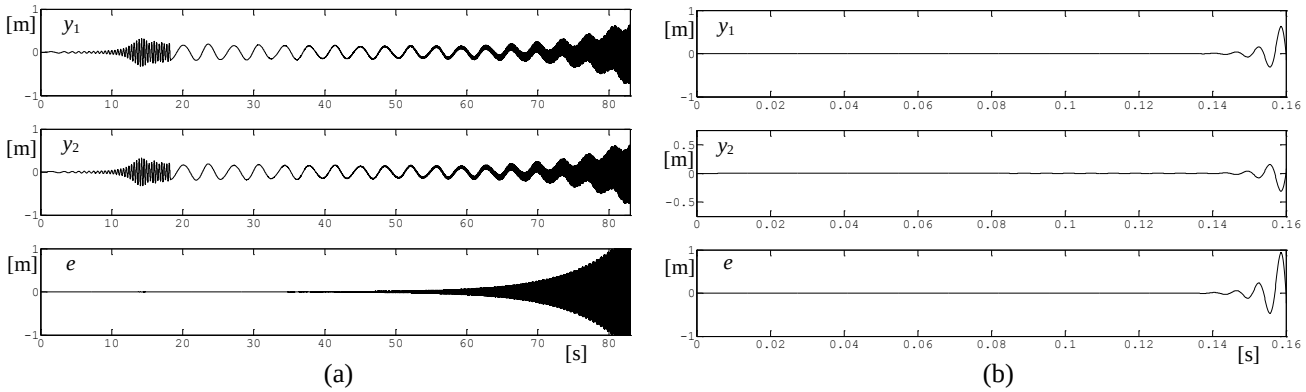

(a) (b)

Fig. 15 Σ_{HS} ; τ = 0.003 s: $\{\Sigma_1, \Sigma_2\}$ responses $\{y_1, y_2\}$ and the error $e = y_1 - y_2$.
(a) Case 2 (b) Case 3

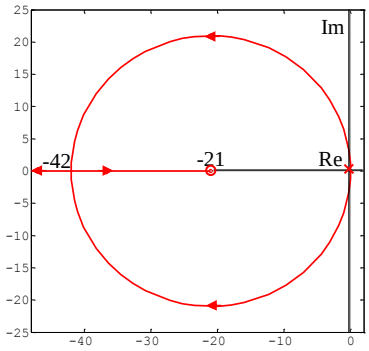

Fig. 16 Σ_{DSS} scheme roots' loci for a varying actuator constant, a; valid for all mass ratios.

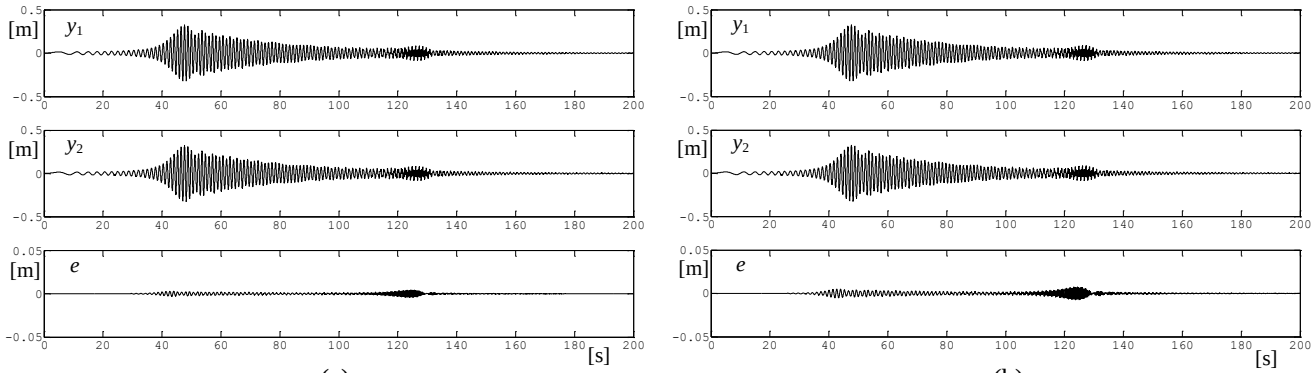

Fig. 17 Σ_{DSS} case 1: $\{\Sigma_1, \Sigma_2\}$ responses $\{y_1, y_2\}$ and the error $e = y_1 - y_2$. (a) $a = 30\ s^{-1}$ (b) $a = 25\ s^{-1}$

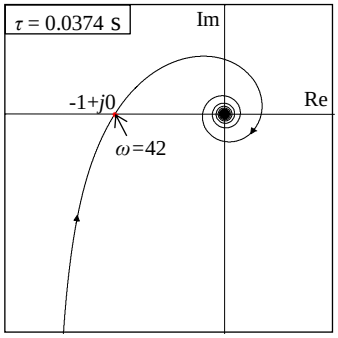

Fig. 18 Σ_{DSS} scheme polar plot of $H(j\omega)$.

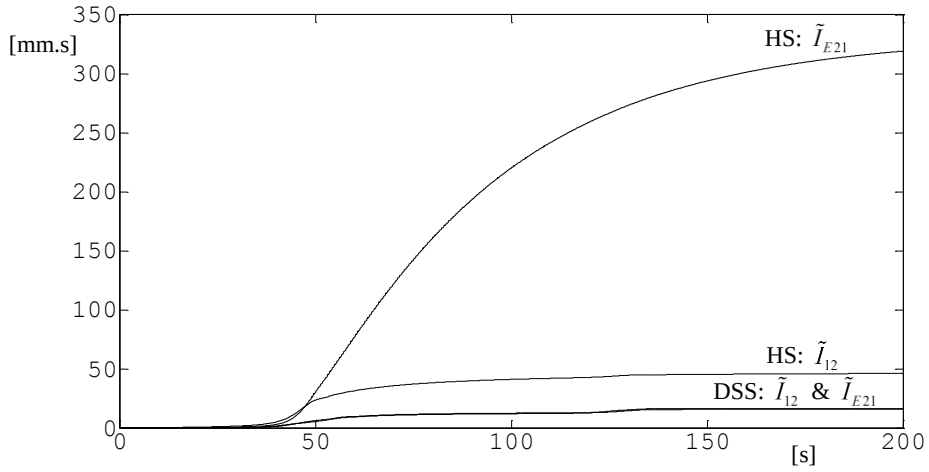

Fig. 19 Mean performance index time-trajectories for the Σ_{HS} and Σ_{DSS} schemes

Test Conditions (Italics indicate nominal parameters. Unlisted parameters are also nominal)			**Performance Indices**			
			Σ_{HS}		Σ_{DSS} (Σ_{USS})	
Case	a [s^{-1}]	τ [ms]	I_{12} [mm.s]	I_{E21} [mm.s]	I_{12} [mm.s]	I_{E21} [mm.s]
1	*42*	*0*	0.0	1.8	0.0	1.8
1	30	*0*	77.7	798	12.5	12.1
1	25	*0*	Unstable		21.4	21.2
2	30	*0*	49.5	24.7	16.2	9.81
3	30	*0*	39.6	296	22.8	22.7
3	130	*0*	Unstable		36.3	37.7
1	*42*	3	17.6	159	3.99	3.81
1	*42*	16	Unstable		22.1	21.5
2	*42*	3	Unstable		5.27	4.70
3	*42*	3	Unstable		7.44	7.69
3	*42*	3			(7.44)	(7.69)
3	*42*	3			(7.41)	(7.80)

Table 1 Performance indices I_{12} and I_{E21} for all stable tests.